8-2021

Effects of Pillar and Sealing Design on thermal and Mechanical Performance of Vacuum Insulated Glazing

Wenyuan Zhu
wzhu15@vols.utk.edu

To the Graduate Council:

I am submitting herewith a thesis written by Wenyuan Zhu entitled "Effects of Pillar and Sealing Design on thermal and Mechanical Performance of Vacuum Insulated Glazing." I have examined the final electronic copy of this thesis for form and content and recommend that it be accepted in partial fulfillment of the requirements for the degree of Master of Science, with a major in Mechanical Engineering.

Seungha Shin, Major Professor

We have read this thesis and recommend its acceptance:

Seungha Shin, Kenneth D. Kihm, Wei Wang

Accepted for the Council:
Dixie L. Thompson

Vice Provost and Dean of the Graduate School

(Original signatures are on file with official student records.)

Effects of Pillar and Sealing Design on Thermal and Mechanical Performance of Vacuum Insulated Glazing

A Thesis Presented for the

Master of Science

Degree

The University of Tennessee, Knoxville

Wenyuan Zhu

August 2021

ACKNOWLEDGMENTS

Here is my sincere appreciation to my supervisor Prof. Seungha Shin, for all his self-giving patience and guidance. And my great thanks to my parents and friends who always bring me brightness in my difficult time.

ABSTRACT

Vacuum insulated glazing with a low-emittance coating has a great market potential as an effective transparent insulator. The thermal insulating performance of VIG is determined by its design, including material selection and configuration of different components. Thermal conductance of the vacuum gap, as a transport bottleneck, is one of the primary factors controlling the thermal transport across VIG. In particular, since support pillars and sealings provide the main thermal transport channels across the vacuum gap, increasing the pillar and sealing thermal resistance is a key strategy for effective thermal insulation, while maintaining the vacuum space and mechanical strength of VIG. In this research, the effects of various design parameters of pillar and sealing on the VIG thermal and mechanical performance were comprehensively investigated and discussed through the finite element method (FEM), along with experimental validation and analytical calculation. The results from the different approaches agree within 4%, providing confidence in the reliability of the employed approaches. The pillar design parameters, especially the height, shape, spacing, and arrangement of the pillars, showed significant effects on the thermal performance of VIG, the smaller contact area for horizontal pillars can effectively decrease the heat loss by more than 30%. An equation of pillar thermal performance was developed and presented. Sealing with flexible materials and sintered glass frits were tested in this work, both performed great performance in airtightness, but glass frits showed the limitation in the tensile test. Details of *U*-value effect and heat flux distribution of seal were analyzed and presented using FEM. Through this research, the guidance and suggestions for enhancing VIG performance through an optimized design of pillar and sealing are discussed.

TABLE OF CONTENTS

LIST OF TABLES

LIST OF FIGURES

CH 1. INTRODUCTION

1.1 Vacuum Insulated Glazing

Window plays a significant role in the current human building environment, which only take up between 10-15% of a home's total surface area that is exposed to outside temperatures, but account for as much as 30% of the heat lost in a home[1, 2]. Against the backdrop of continuously rising energy costs, windows are identified as critical weak spots, and therefore developments in the field of vacuum insulated glazing (VIG), which can significantly reduce heat loss, are of great importance[2, 3]. VIG is an assembly consisting of at least two glass panes that are separated by an array of pillars, hermetically sealed along the periphery, in which the gaps between the glass planes are under vacuum. For VIG to have a higher thermal resistance (*R*-value) than conventional glazing, the vacuum pressure needs to be below 0.133 N/m^2 (10^{-3} Torr) [4]. Vacuum glazing is considered to be a promising technology to replace single pane glazing in window products to minimize heat loss and maintain high visible transmittance. Since the first introduction of the VIG concept in 1919 [4] and its first successful fabrication in 1989 [5], researchers in the public and private sectors have worked to improve VIG, especially focusing on its thermal insulating performance [6-11], durability, and cost.

After 1924, in which year the first VIG patent was granted, a steady and continuous stream of patents in the area of vacuum insulate glazing was generated, which indicated the high level of interest in this area[12]. However, the way of development comes with considerable difficulty in fabricating the VIG system[12], the process technology is old and each component of vacuum glass has the potential to bring the difference to the overall

performance of VIG system, for example, the size of glass pane, the materials of seal, the shape of support pillar and so on. It takes many years for research to determine the best way to fabricate the vacuum insulated glass[2, 13, 14] while only a few research were started to investigate the best design for vacuum insulated glass and find out the correlations among different design parameters.

The description of VIG system in a building was shown in Fig. 1.1, the vacuum insulated glass is usually applied in the city-building system to play a significant role in reducing heat transfer. The glass pane has red color in the figure is facing the outdoor environment while the blue one is facing the indoor environment; the gap design provides a huge effect in reducing the thermal transfer from outdoor to indoor by employing a vacuum inside. Without most of the thermal conductors, the radiation thermal transfer becomes the first consideration in improving the performance of VIG. In order to solve this primary consideration, low-emittance (Low-E) coating was created and applied into the VIG system[15], which can reach the value of emissivity as lower as 0.018 and reflect most of the energy.

Since the radiation thermal transfer had been significantly reduced by Low-E technology, the primary consideration of reducing thermal transfer was moving to the components of gap, especially the support pillar and seal (shown in Fig. 1.2). To be specific, the support pillars were made of several parallel solids that have a regular arrangement, which usually used cylinder in small radius and lattice style arrangement; on the other hand, primary seal and secondary seal are two components of the seal design, for some vacuum window, they could be considered as one single seal together, others were using different

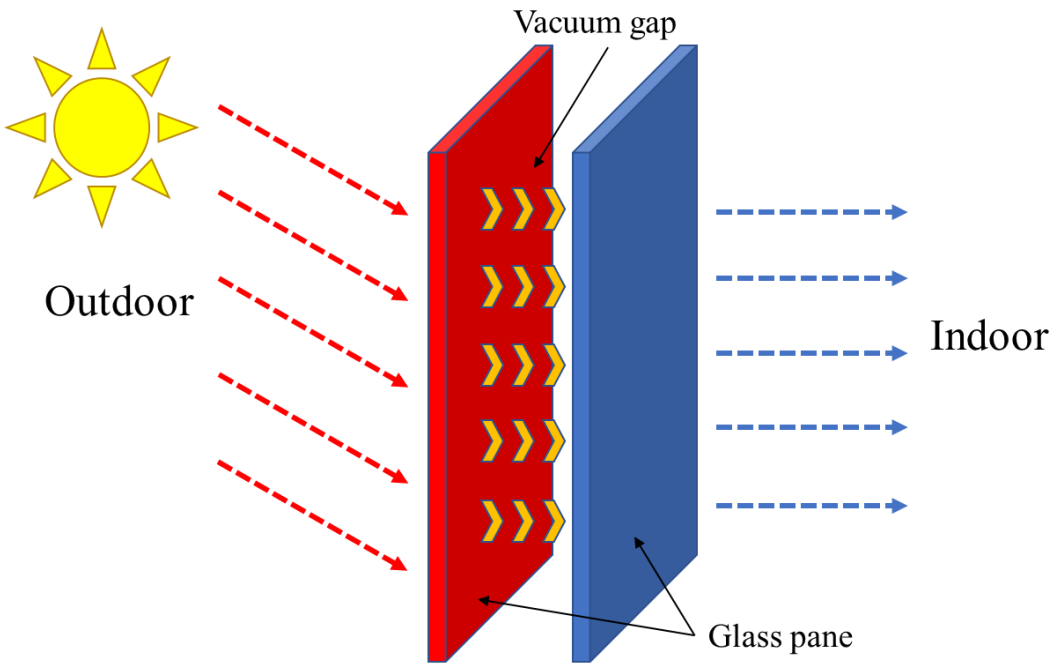

Figure 1.1. Simplified system of VIG, two glass panes with different color faced outdoor and indoor environment, respectively, the gap between two glass panes was vacuum, support pillar and seal are ignored in this simplified system figure.

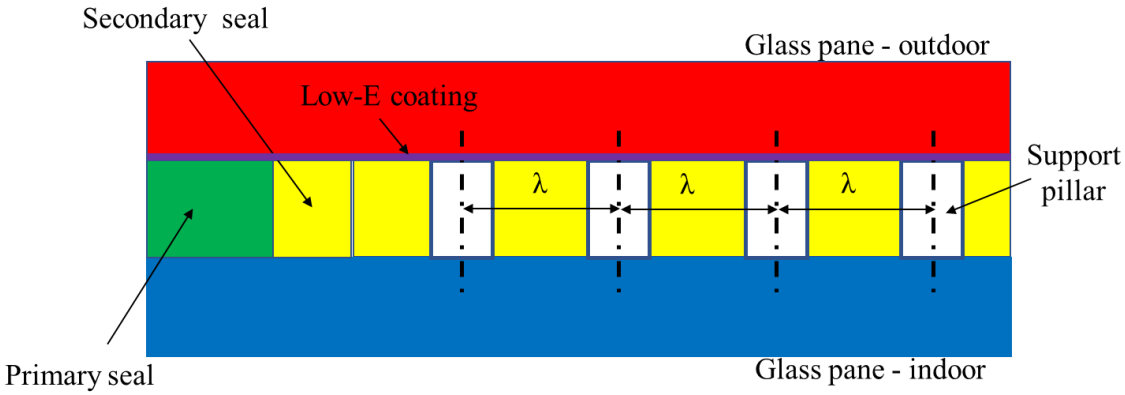

Figure 1.2. Detail of vacuum gap between two glass panes in part of the VIG system, including indoor and outdoor glass pane; Low-e coating; primary and secondary seal and support pillars.

materials for primary and secondary seal or adding additional layers into the seal; the Low-E coating was applied in the inside surface of the outdoor glass pane, while the indoor glass pane was keeping the same. The parameters of gap design including pillar and seal generally became the key factor in improving thermal and mechanical performance of VIG.

Besides thermal performance, mechanical performance is another index that cannot be ignored. With the vacuum employed in the gap of VIG, stress resistance could be a problem during the VIG working process because of the atmospheric pressure outside the window. In that case, the pillar and seal would be the main source of resistance to support the VIG product, therefore, investigating the correlation between gap (pillar and seal) design and mechanical performance of VIG to enhance the overall mechanical performance and guarantee the reliability and stability of vacuum insulated glass is necessary.

1.2 Pillar and Sealing Design

From the discussion above, the gap of vacuum insulated glass, which including the seal, pillar, and radiation, plays a significant role in enhancing the thermal performance of VIG. Since the low-E coating has been widely applied into currently VIG products to reduce the effect of radiation transfer, the focus in this work was put on the sealing and pillar design to enhance the thermal and mechanical performance of VIG.

To be specific, both pillar and seal have several design parameters that need to be considered like height, volume, shape, arrangement, etc. Since the 1980s, researcher was trying to change some of these parameters to find the correlation between parameters and VIG performance that can help improve the VIG product[15-19]. However, due to the

limitation of test technology and the expensive source in experiments, the progress kept slow until the computational method been general applied in this research field.

Thanks to the no materials consuming and easily controllable parameters in the computational test, the computational method brought more accuracy and efficiency to the investigation of VIG products especially the finite element method[20-23]. However, most of the research are only focus on one or two parameters of VIG design separately, the simulation cases are limit in number and the correlation between several parameters is still unclear. It is necessary to comprehensively consider several parameters together which can make a more reliable result for our investigation. On the other hand, the method in those research was also limit in number, if consider the validity and accuracy of results, it is better to have several methods together than just one single method.

In this work, we investigated the effects of various pillar parameters and sealing parameters on the mechanical performance and thermal insulation performance of VIG, using 3D FEM coupled with experimental validation and analytical calculation. Based on this analysis, we evaluate the significance of each pillar and sealing design parameter in VIG, try to improve the overall thermal performance of VIG system while maintaining safety and reliability in mechanical performance.

1.3 Thesis Outline

The investigation process was shown in Fig. 1.3. The goal of this thesis is to figure out the correlation between pillar & sealing design and the performance of VIG, investigate the effects of several parameters comprehensively by applying FEM, experiment, and analysis methods, improve the mechanical and thermal performance of VIG.

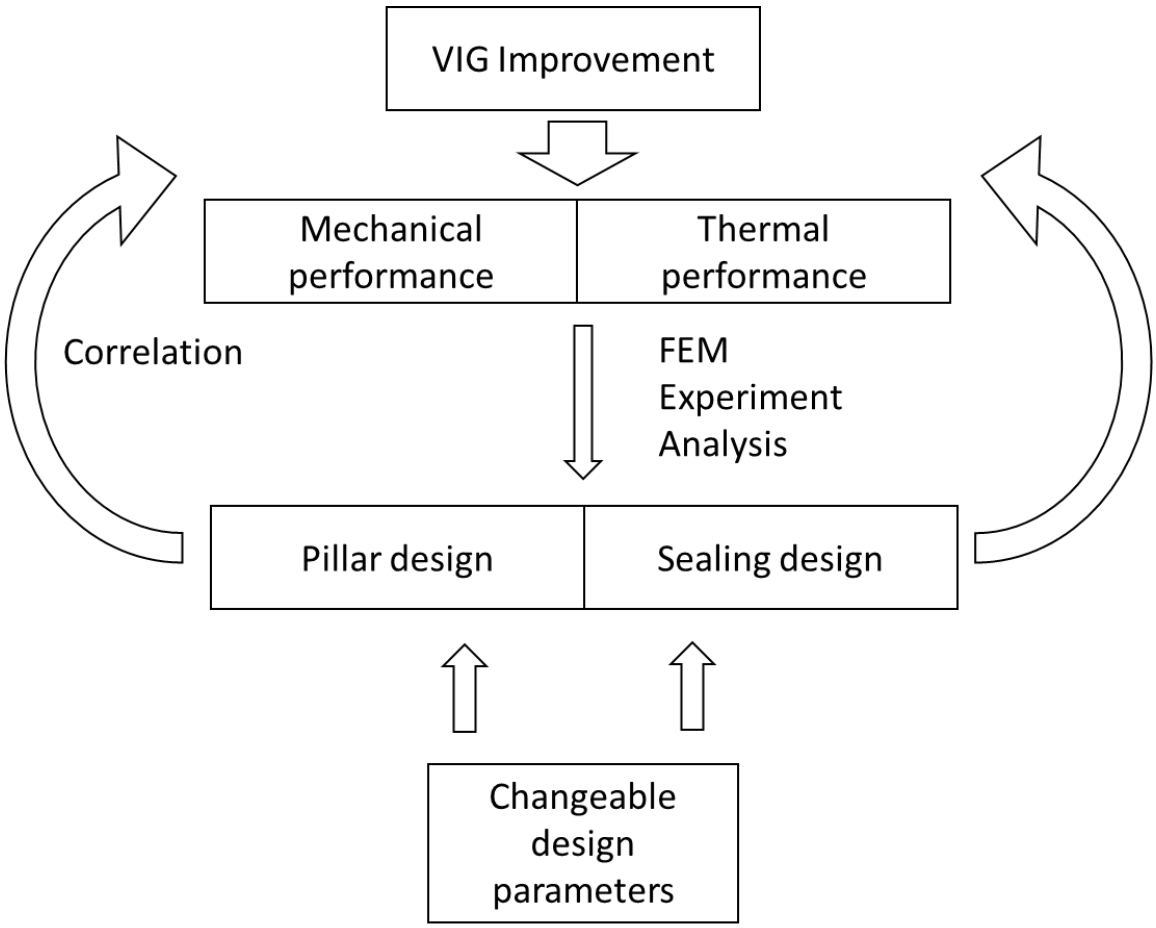

Figure 1.3. The investigation process of effects of pillar and sealing design on thermal and mechanical performance of VIG in this work.

Chapter 2 presents the detailed work of pillar design effect investigation; several pillar parameters are comprehensively tested and discussed in this chapter. The finite element analysis was the main method to investigate the influence of different pillar design parameters. A professional experiment system in Oak Ridge National Laboratory was responsible for the experiment process in this chapter, which was to guarantee the reliability of our FEM model and valid the influence of pillar design on thermal and mechanical performance. Besides, analytical method would be another method to validate the result from FEM, the comparison between these two methods is discussed in detail, a developed analytical equation is presented based on current work.

Chapter 3 discusses the effect of different sealing design parameters by applying FEM and experiment methods. Two different types of seal, flexible material and glass frit, were test and compared to optimize current VIG products. The correlation between sealing design and performances of VIG was studied and discussed.

Chapter 4 concludes the work presented in this thesis and suggests a possible extension of this study for future work, specifically for further improvement of vacuum insulate glazing thermal performance and mechanical performance.

CH 2. EFFECT OF PILLAR DESIGN

Note: Chapter 2 is a modified version of the submitted paper: **Wenyuan Zhu**, Suhong Zhang, Seungha Shin, Sarma Gorti, Bipin Shah, Mahabir Bhandari*, and Pooran Joshi, "Effects of Pillar Design on the Thermal Performance of Vacuum Insulated Glazing" The Journal of Construction and Building Materials, Under Review (2021)

2.1 Introduction

Enhancing the effective thermal insulation requires optimizing the design of the gap between the glass panes, consisting of vacuum and support pillars, since it provides a thermal transport bottleneck for the overall heat transfer. Several parameters of the pillar array have been investigated separately, highlighting their considerable influence on the thermal performance of the vacuum glazing [24-26]. These studies have shown the important role played by the thermal conductance of the gap region, as well as the effect of the edge in relation to the gap, on the thermal performance of the VIG. However, these efforts have been mainly concerned with cylindrical pillars with specific sizes and spacings, as well as specific pillar materials. This research seeks to improve the VIG thermal performance through a comprehensive parametric study involving various parameters related to the gap design, including the investigation of alternate pillar shapes. The ultimate objective is to develop sufficient insights into the combined influence of these different parameters, that could then be used to optimize the design of the VIG.

It is expensive and technologically challenging to explore all the possible VIG design parameters and comprehensively examine their effects. Thus, computational simulations have been widely used as a more economical and effective way to study the VIG thermal performance. Among simulation approaches, the finite element method (FEM)

has been widely used for thermal and structural analysis of VIG due to its accuracy and efficiency [27]. The thermal performance of VIG can be evaluated by two-dimensional (2D) FEM modeling [22, 28], which enables simpler and faster analysis; however, the details of thermal bridges, such as pillars, cannot be addressed [29]. For the design and analysis of VIG, three-dimensional (3D) FEM is employed, as it provides greater accuracy and can include the detailed features [30]. While the selection of materials for each component has been focused on in previous studies for the VIG enhancement, the effects of structural parameters along with thermal performance and their underlying mechanisms have been relatively unexplored. Specifically, the pillar design dominates the gap conductance, directly affecting the overall heat transfer of VIG. Thus, the effects of various pillar design parameters, such as pillar shape, contact area, height, and arrangement, in addition to their thermal conductivity, should be comprehensively evaluated for an optimized VIG design.

In this chapter, we investigated the effects of various pillar parameters on the mechanical performance and thermal insulation performance of VIG, using 3D FEM coupled with experimental validation and analytical calculation. Based on this analysis, we evaluate the significance of each pillar design parameter in VIG, and the validity of the theoretical formula for the enhancement of the VIG thermal analysis.

2.2 Methodology

2.2.1 System Configuration of Computational Modeling

The modeled VIG consists of two parallel glass panes, array of support pillars in the gap between the two glass panes, and two layers of edge seal (primary and secondary seals) along the periphery of the glass in the gap, as illustrated in Fig. 2.1a. The modeled

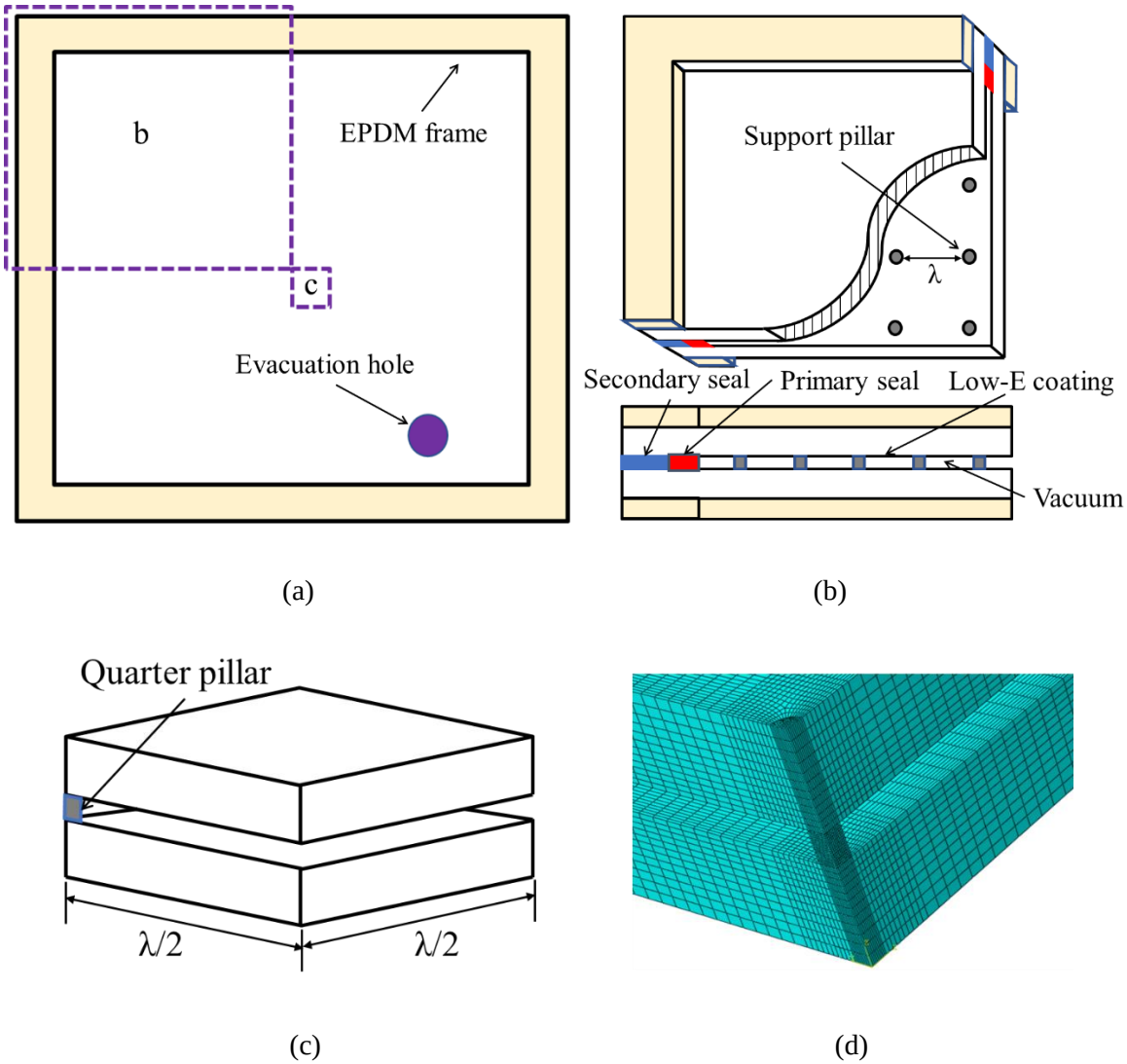

Figure 2.1. (a) Configuration of VIG window for FEM models. (b) A quarter VIG model including all the details of the peripheral region/frame. (c) A quarter unit-cell representing infinite VIG was employed to study the pillar effects. (d) Finer mesh was used in the vicinity of the pillar.

VIG is assumed to have the top and bottom glass panes facing the outdoor and indoor environment, respectively. Both glass panes have a dimension of 1,000 mm × 1,000 mm × 3 mm, and a low-emittance coating with an emissivity of 0.018 was applied to the inner surface of the top glass.

To simulate the VIG window installation, on the outside edge surfaces of both glass panes, ethylene propylene diene monomer (EPDM) rubber with a low thermal conductivity (k_{EPDM} = 0.25 W/m-K) was added to cover the side frame of VIG with thermal insulation. In the gap the model assumed 0.133 N/m^2 (or 10^{-3} Torr) for the vacuum pressure (P_{vac}), which is close to that used in conventional VIG products. Under a benchmark or baseline condition for the study of pillar effects, cylindrical pillars with height of 1 mm (h = 1 mm) and radius of 0.5 mm (r = 0.5 mm) were placed in the gap and arranged in a square array with 50-mm pillar spacing (λ = 50 mm). Primary seal with thickness of 1.4 mm and width of 5 mm, and secondary seal with thickness of 1 mm and width of 7 mm, were set to adhere to each other at the edge of the glass panes. Material properties for the employed FEM model are summarized in Table 1. (Note: in the actual construction of the VIG, primary and secondary seals were used which have similar properties).

Due to the symmetry of the modeled window, the FEM modeling of a quarter section of the full window, i.e., 500 mm × 500 mm (Fig. 2.1b), can accurately represent the whole VIG. This quarter VIG model includes all the details of VIG components, including the seals and EPDM, which enables more accurate mechanical and thermal analysis. In addition, to focus on pillar effects on thermal transport, a quarter of one-unit cell, consisting of (λ/2) × (λ/2) section (λ is pillar space in mm) of glass panes and a quarter

Table 1. Physical properties of VIG components

Material	Density (g/cm^3)	Elastic Modulus (GPa)	Poisson's ratio	Conductivity (W/mK)	Specific heat (J/kg-K)	Expansion Coeff. ($\times 10^{-6}$ /K)
EPDM	1.4	2.5	0.47	0.25	1000	80
Glass	2.5	73	0.22	1	800	8.6
Pillar	3.5	280	0.22	1	800	8.6
Primary Seal	2.5	75	0.22	1	800	20
Secondary Seal	1.54	3.5	0.33	0.35	1000	50

pillar, was modeled as shown in Fig. 2.1c. This smaller system model allows for finer mesh setups, which lead to higher accuracy, reducing the computing cost in FEM, although this model represents an infinite VIG and excludes the consideration of frame, seal, etc. Through the comparison between a quarter window model and a quarter unit cell model, the contribution of a pillar-glass unit to overall heat transfer can be evaluated.

Generating a proper mesh is important to achieve efficient and accurate calculations in FEM. Smaller element size leads to more accurate solutions in general, as the numerical errors in the FEM approximations decrease, while requiring more computing resources due to a larger number of elements. Regions with a large variation of properties, such as near the interface between two different materials, need more elements. To obtain the optimal balance between accuracy and computing cost, various meshing conditions were tested and confirmed through mesh-convergence studies [31]. The final element sizes were chosen to be smaller than 10^{-4} mm^3, and the element size in interfacial regions is 2% - 12.5% of other parts, as shown in Fig. 1d. In this research, all the FEM simulations for thermal transport and mechanical analysis were conducted using the commercial FEM program ABAQUS [32, 33].

To examine the effects of pillar design on the thermal performance, several pillar parameters, which include the thermal conductivity, spacing, alignment, height, volume, contact area, and shape, were investigated, deviating from the benchmark conditions. Our simulations examined the thermal conductivity of pillar (k_{pa}) ranging from 1 to 999 W/m-K and the spacing (λ) from 15 to 60 mm in a square array. Vertically aligned cylinder with 1-mm height and 1-mm diameter (Fig. 2.2a) was basically employed as a benchmark, but

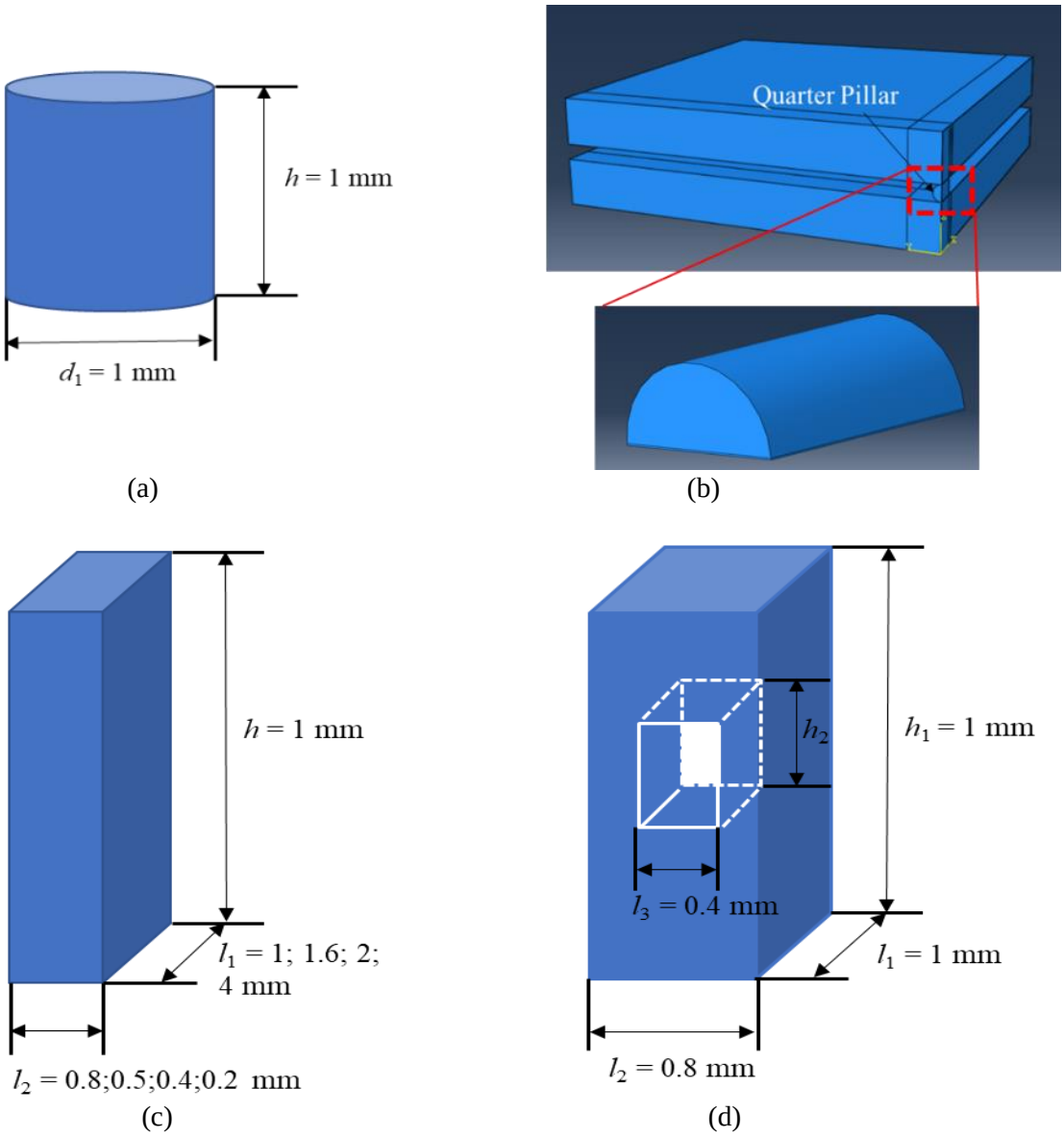

Figure 2.2. (a) Benchmark geometry of cylindrical pillar. (b) Quarter unit cell (25 mm × 25 mm) model with a horizontally placed cylindrical pillar. (c) Various geometries of pillars including rectangular parallelepiped and hollow rectangular parallelepiped pillar.

horizontal cylinders were also simulated (Fig. 2.2b). For both horizontal and vertical cylinders, the axial length varied from 1 to 3 mm. To study the influence of pillar volume, shape, and pillar-glass contact area, different geometries of pillars, including rectangular parallelepiped, hollow rectangular parallelepiped, etc., were also examined, as depicted in Fig. 2.2c. We also considered a model named Sample#1, which has similar geometry features to the benchmark case, and was mainly used for validation against experimental data.

2.2.2 Computational Analysis of VIG Windows

1) FEM Modeling

As vacuum is introduced within a VIG window, the pressure difference between the vacuum and atmospheric pressure deforms the glass panes. Under severe glass deformation, the two glass panes can be in contact, creating a new conduction path, which brings a sharp increase in *U*-value (overall heat transfer coefficient). To prevent the glass from collapsing under vacuum pressure, very small size pillars are placed at regular intervals between the glass panes. These pillars also provide structural support under different stresses caused in the cavity due to service conditions. To confirm that the modeled VIG is not significantly distorted because of the pressure difference, structural analyses (using FEM simulations) were conducted with the VIG model in Fig. 2.1b. Symmetry boundary conditions were applied to the two sides of the model that correspond to the centerline along the *x* and *y* directions of the full VIG, while the nodes along the top and bottom surface of the EPDM frame were constrained to have zero displacement. Frictionless contact was assumed between each pillar and the top glass pane, and a cohesive

interface with a stiffness of 10^6 N/mm^2 was assumed between each pillar and the bottom glass pane. One atmosphere pressure load was directly applied to the outside surfaces of both glass panes. Heat transfer coefficients on the outer surfaces of outdoor and indoor glass panes (C_{out} and C_{in}) were set to 29.41 W/m^2-K and 6.67 W/m^2-K, respectively, (these boundary conditions were taken in accordance with ASTM C1199[34] testing procedure). Assuming extreme weather conditions, 60°C and -30°C were used for the outdoor temperatures, while the indoor temperature was fixed at 23°C to simulate ASTM E2188 and E2190[35, 36] durability test conditions.

After confirming that the mechanical deformation was insignificant even under extreme service conditions, the thermal performance of the VIG, which is characterized by the overall heat transfer coefficient (U, W/m^2-K), was examined. Simulations for thermal analysis employed a standard thermal condition of -18°C for outdoor and 21°C for indoor under a steady-state condition. The U-value was calculated as

$$U = Q/ (A_{eff}\, \Delta T), \tag{1}$$

where Q is the overall heat transfer rate of the VIG model, A_{eff} is the effective area for VIG model (using the top/bottom view area of the model), and ΔT is the temperature difference between the outdoor and the indoor. Q is calculated by integrating heat flux over effective surface area ($Q = \sum q_i A_i$), which can be obtained from the FEM simulation output.

2) One Dimensional Thermal Analysis

The overall heat transfer coefficient (U)[10] can also be calculated using 1D thermal analysis with theoretical and empirical formulas for thermal resistances of each component as shown in Fig. 2.3. This analytical calculation provides a quick estimation of thermal

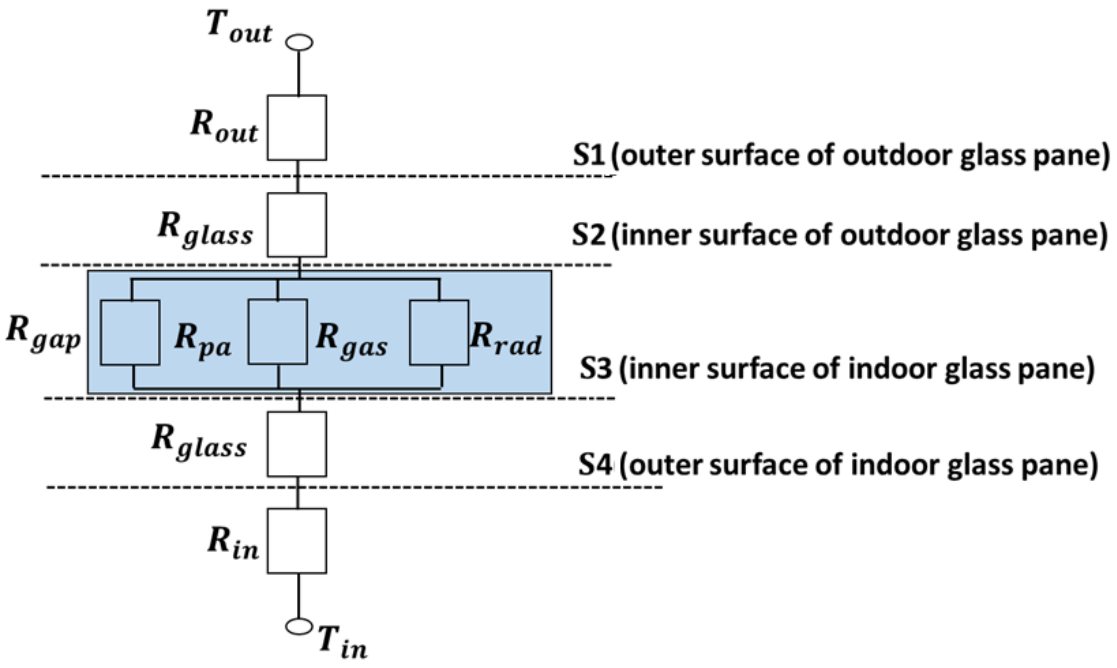

Figure 2.3. Thermal circuit diagram for the modeled VIG system.

performance and facilitates the analysis of the VIG thermal transport, as the contribution of each VIG component can be separately evaluated. Based on the indoor and outdoor temperatures, and heat flow across the glass/surroundings interfaces (sealants), glass panes, and vacuum gap, the thermal resistances corresponding to each heat transfer medium can be considered in series, so that the *U*-value is given as

$$U = \frac{1}{R_{out}+R_{in}+2R_{glass}+R_{gap}}, \tag{2}$$

where R_{out}, R_{in}, R_{glass} and R_{gap} represent the areal thermal resistances of outdoor and indoor surface heat transfer, glass conduction, and heat transfer through the gap region, respectively. R_{out} and R_{in} are the reciprocals of the heat transfer coefficients on the two outer surfaces (S1 and S4 in Fig. 2.3), i.e., $R_{out} = 1/C_{out}$ and $R_{in} = 1/C_{in}$.

The thermal resistance of conduction across the glass pane (R_{glass}) is t_{glass}/k_{glass}, where t_{glass} is the thickness of the glass, and k_{glass} is the thermal conductivity of the glass. The thermal resistance to heat transfer across the gap (R_{gap}) includes contributions from R_{rad}, for the radiation between the two inner surfaces of top and bottom glass panes (S2 and S3 in Fig. 2.3), R_{gas}, for the conduction through low-pressure gas (vacuum) and R_{pa}, for conduction through the pillars. Thus, three resistances for the radiation, gas conduction, and pillar conduction, need to be considered in parallel as in Fig. 2.3, and then, the resistance across the gap (m^2-K/W) is given as

$$R_{gap} = \frac{1}{{R_{rad}}^{-1}+{R_{gas}}^{-1}+{R_{pa}}^{-1}}. \tag{3}$$

Thermal resistance of low-pressure gas conduction can be calculated using the gas kinetic theory, given by [37]

$$R_{gas} = \left[\bar{\alpha}\left(\frac{\gamma+1}{\gamma-1}\right)\left(\frac{R}{8\pi MT}\right)^{\frac{1}{2}} P_{vac}\right]^{-1} \text{ and } \bar{\alpha} = \frac{\alpha_{S2}\alpha_{S3}}{\alpha_{S3}+\alpha_{S2}(1-\alpha_{S3})A_{S2}/A_{S3}}, \quad (4)$$

where A is the area, α is the accommodation coefficient of the gas molecules, and the subscripts S2 and S3 refer to the inner surfaces of outdoor glass pane and indoor glass pane, respectively. The α parameter depends on the temperature, surface conditions, etc., and for the present configuration and conditions, we employed α_{S2} and α_{S3} = 0.79 and $\bar{\alpha}$ = 0.653. In Eq. (4), γ is the specific heat ratio of air (γ = 1.4 near room temperatures), M is the air molar weight (M = 28.97 kg/kmol), R is the molar gas constant (R = 8.314 J/mol-K), and P_{vac} is the pressure of the gap (P_{vac} = 0.133 N/m^2). T is the average value of inside surface temperatures for outdoor glass (T_{S2}) and indoor glass (T_{S3}). The radiation resistance is given by [38]

$$R_{rad}{}^{-1} = \frac{1}{\varepsilon_{s2}{}^{-1}+\varepsilon_{s3}{}^{-1}-1}\sigma_{SB}\frac{T_{s2}{}^4-T_{s3}{}^4}{T_{s2}-T_{s3}}, \quad (5)$$

where σ_{SB} is the Stefan-Boltzmann constant and ε_{S2} and ε_{S3} are the radiation emissivities of inner surfaces of top and bottom glass panes (S2 and S3). While ε_{S3} is 0.84, the inner surface of top glass with a low-emissivity coating has ε_{S2} equal to 0.018. The resistance due to pillar conductance[38, 39] was calculated using

$$R_{pa}{}^{-1} = C_{pa} = \frac{2k_{glass}r}{\lambda^2\left(1+\frac{2k_{glass}h}{k_{pa}\pi r}\right)}, \quad (6)$$

where λ, r, h, and k_{pa} are the spacing, radius, height, and thermal conductivity of the pillar, respectively, and k_{glass} is the thermal conductivity of the glass pane. Considering the important roles played by the pillar height and pillar thermal conductivity, this equation captures the effects of not only pillar spacing and pillar radius but also pillar height and

thermal conductivity. However, it is limited in its applicability to the analysis of cylindrical array of pillars.

Results from FEM simulations were validated by comparing them with experimental results on a VIG sample as well as analytical calculations using WINDOW[40] software program formulas and ASTM C 518[41] test procedure. WINDOW software, which was developed by Lawrence Berkeley National Laboratory and has been serving industries, the public, and policymakers with informed research for 50 years, was used as the primary indicator and validation method[40]. In this work, results from both FEM and WINDOW were compared for validation.

2.2.3 Experiment

Center-of-glass thermal transmittance value of a VIG sample (Sample#1) was measured in accordance with ASTM C 518 test procedure and following the ISO 19916-1_18[42] procedure at Oak Ridge National Laboratory. The VIG assembly consists of two panes of glass (one clear and one low-E coated), separated by an array of cylindrical pillars and sealed along the periphery. Fox 670 Heat Flow Meter apparatus (Fig. 2.4a) was used for the measurements. The VIG unit is placed between two buffer plates (Fig. 2.4b) of known thermal conductivities in the FOX 670 apparatus in horizontal position. To obtain the VIG thermal resistance, the buffer plate resistance values were subtracted from the overall measured resistance value. The mean temperatures of heating and cooling plates were fixed at 17.5°C and 2.5°C, respectively. Construction details of the sample details is listed in Table 2. The measured VIG sample results were used for the validation of the FEM simulations.

Table 2. Configuration of Experimental VIG

Parameters	VIG
Glass thickness (mm)	4
Vacuum gap/Pillar height (mm)	0.305
Pillar radius (mm)	0.305
Pillar space (mm)	40
Emissivity Coating	0.84/0.036
Pillar conductivity (W/m-K)	16
Vacuum thermal conductance (10^{-3} W/m^2-K)	1.0679
VIG glass size (mm)	508 × 508

(a) (b)

Figure 2.4. (a) FOX 670 appartus used for VIG measuremnets, (b) two buffer plates of known conductivity

2.3 Results and Discussion

2.3.1 Mechanical Effect of Pillar Parameters

Using thermo-mechanical simulations with a quarter window model, the displacement in the *z*-direction, i.e., perpendicular to glass surface, was calculated as presented in Figs. 2.5a-2.5d. Both hot and cold outdoor cases show a larger *z*-direction displacement in the center region of the window. The direction towards outdoor is defined as the positive *z*-direction of the glass. For $T_{out} < T_{in}$, the *z* displacement appears in the negative direction with a maximum value of 0.59 mm, while for $T_{out} > T_{in}$, the displacement is towards the outdoor with a maximum value of 0.10 mm. According to glass mechanical properties test[43], the maximum value of *z*-direction displacement is within a safe range. Additionally, the maximum displacement in the *x*-direction and *y*-direction is approximately two times smaller than in the *z*-direction.

The stress distribution was evaluated along a path across the two glass panes and a pillar in the center area for the case with $T_{out} > T_{in}$, as shown in Fig. 2.5e. Normal stress distributions in *x* and *y* directions are almost identical due to the symmetry; both display significant changes across the glass-pillar interface, and the maximum normal stresses in *x* and *y* directions are 160 MPa at the interface. In contrast, the maximum normal stress in the *z*-direction (260 MPa) occurs at the middle of the pillar. For the stress distribution in the radial direction of pillar, the maximum normal and shear stresses appear near the rim of the pillar on its top and bottom surface. As the area near the rim has considerably higher stress than the stress in the center of the pillar body in the radial direction, attention needs to be paid when choosing the pillar materials to ensure they can withstand the high stresses.

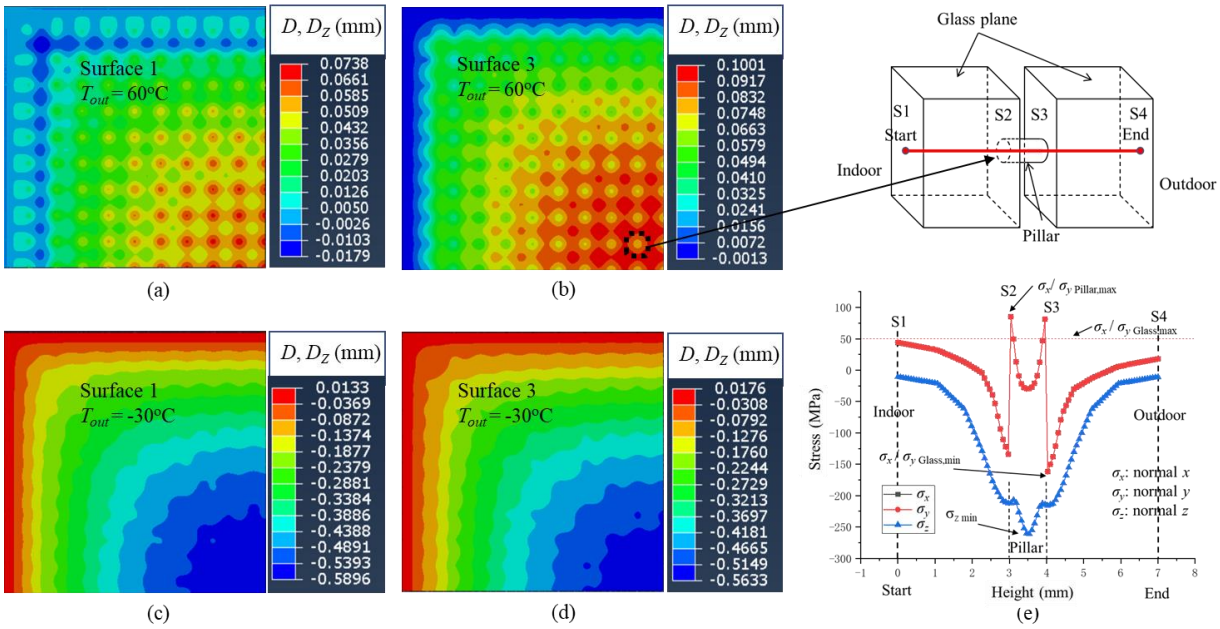

Figure 2.5. (a-d) Glass displacement in the *z* direction with the surface selection in Fig. 2.3. For T_{out} = 60˚C and T_{in} = 23˚C, the displacement (a) on the exterior surface of the outdoor glass (S1) and (b) on the inner surface of the indoor glass (S3). For a cold outside (T_{out} = -30˚C), (c) the displacement on the exterior surface of the outdoor glass (S1), and (d) on the inner surface of the indoor glass (S3). (e) Stress distribution along a path through the indoor glass, a pillar in the center region, and outdoor glass as shown in the schematic above.

To separately observed the stress distribution of pillar as shown in Fig. 2.6, the maximum stresses are appearing near the top and bottom surface ring of the pillar. Some of the points near the ring might have much higher stress than the stress in the center of pillar body. Attention needs to be paid when choosing the materials, in case the unaffordable of these stresses.

Normal x stress has a maximum value about 215.8 MPa; normal y stress has a maximum value about 229.8 MPa; normal z stress has a maximum value about 896.5 MPa; shear xy stress has a maximum value about 39.4 MPa; shear xz stress has a value about maximum value about 112.1 MPa; shear yz stress has a value about maximum value about 111.2 MPa.

2.3.2 Thermal Effect of Pillar Parameters

In the experiment with Sample#1 for the validation of the computational simulation, the thermal conductance between the outer surfaces of the indoor and outdoor glass panes (C_s) was evaluated as it can be more accurately measured. Excluding C_{in} and C_{out} from U, C_s values from the FEM and analytical calculation were determined, using $C_s = 1/[(1/U) - (1/C_{in}) - (1/C_{out})]$ and compared with the experiment. The results from FEM, experiment, and analytical calculation are 0.531 W/m^2-K, 0.548 W/m^2-K and 0.533 W/m^2-K, respectively. The error among these three methods is smaller than 4%, which is acceptable for this validation.

U-value including the surface convection on the glass outside surfaces was calculated from analytical calculations and FEM simulations with the quarter window (Fig. 2.1b) and quarter unit cell models (Fig. 2.1c), varying k_{pa} from 1 to 999 W/m-K, and the

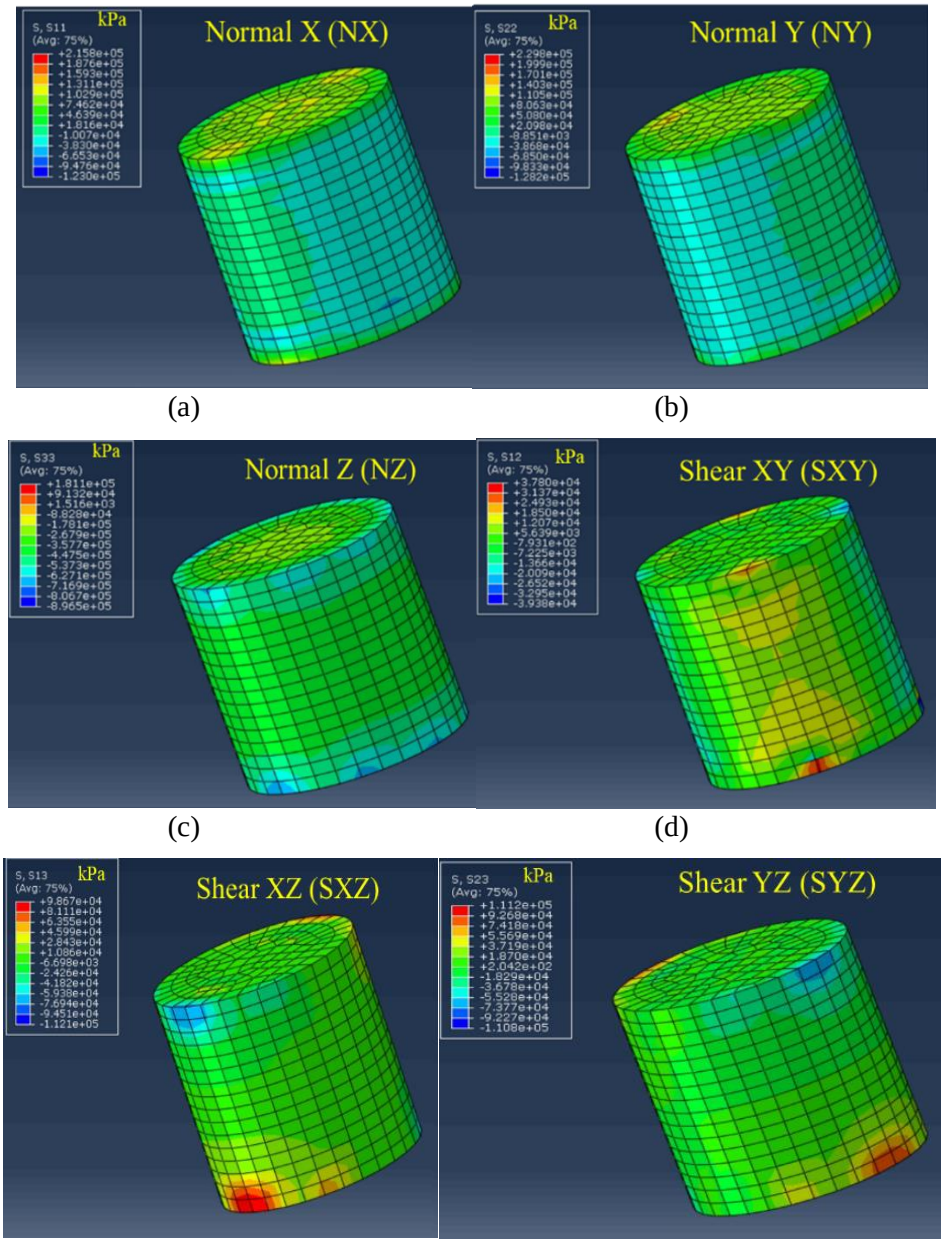

(a) (b)

(c) (d)

(e) (f)

Figure 2.6. Stress distribution of single pillar in different directions. (a) stress disrtibution in normal *x*-direction, (b) stress disrtibution in normal *y*-direction, (c) stress disrtibution in normal *z*-direction, (d) shear stress disrtibution in *xy*-direction, (e) shear stress disrtibution in *xz*-direction, (f) shear stress disrtibution in *yz*-direction

results are presented in Fig. 2.7. Comparison between the results from the quarter window and quarter unit-cell (assuming infinite window) FEM models indicates almost identical *U*-value dependence on various pillar conductivities, except for a shift in the corresponding values. This demonstrates that components in the peripheral region of VIG window, such as frame and sealing, have constant contributions to the overall *U*-value, which justifies the use of quarter unit-cell model for the investigation of pillar effects on VIG thermal insulation. The *U*-value increases with k_{pa}, as expected, and the increase of *U*-value is much more significant at low k_{pa}'s. Specifically, the *U*-value increases by 40% as k_{pa} increases from 1 to 50 W/m-K, which is 24 times larger than the corresponding increase between 50 and 999 W/m-K.

The heat transfer coefficients of the low-pressure gas conduction and radiation in the vacuum gap are 0.107 W/m^2-K and 0.083 W/m^2-K, respectively, independent of k_{pa}. This provides the lower limit of the gap conductance (0.190 W/m^2-K), regardless of the pillar design. With a very low k_{pa}, the heat transfer through low-pressure gas conduction and radiation is comparable to the pillar conduction. According to Eq. (6), the pillar conductance across the gap is more dependent on pillar spacing than k_{pa}, when k_{pa} is much larger than k_{glass}. For k_{pa} higher than 50 times k_{glass}, decreasing k_{pa} can induce only a minor improvement in the thermal insulation performance of VIG. On the other hand, if k_{pa} is comparable to k_{glass}, minimizing k_{pa} has a significant influence on the VIG thermal insulation.

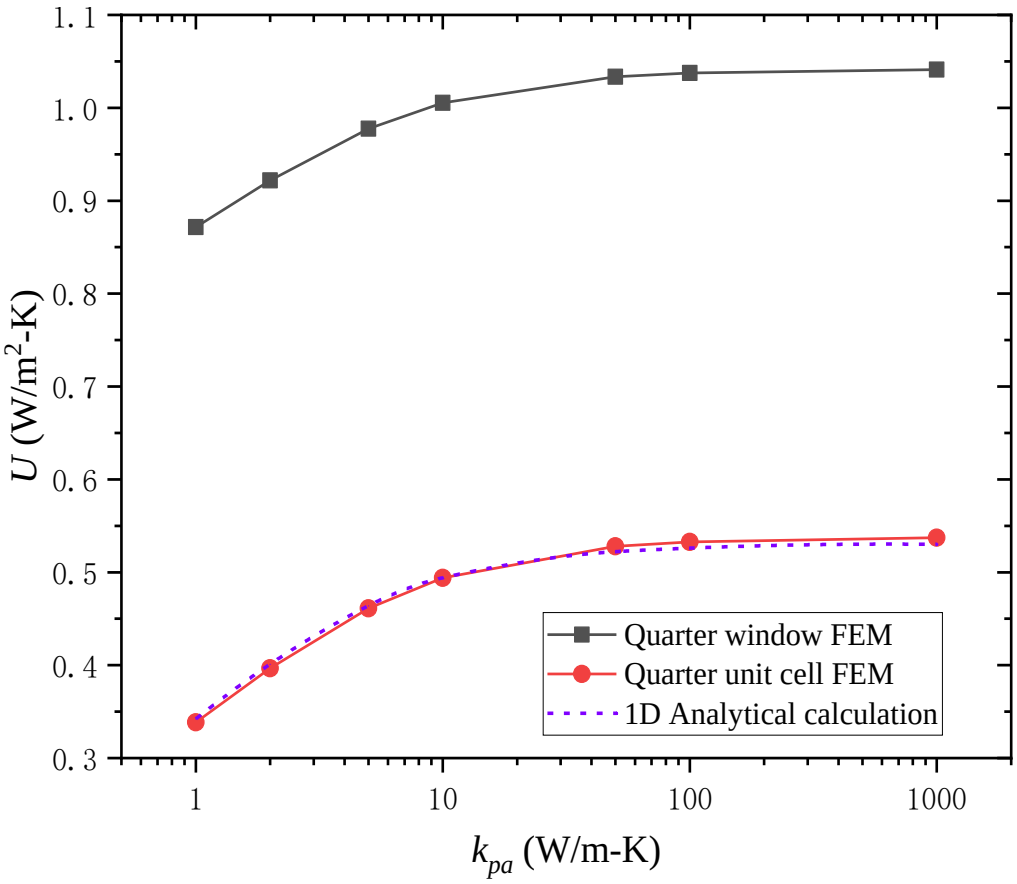

Figure 2.7. *U*-values from 1D analytical calculation (purple, dashed) and FEM simulations with the quarter window model (red, circles) and the quarter unit cell model (black, squares) with respect to the pillar thermal conductivity (k_{pa}).

Pillar Geometry

First, the effect of the pillar height (h) or the gap height was examined using FEM with the quarter unit cell model and varying k_{pa}, and the results are presented in Fig. 2.8a. Increasing the pillar height leads to a decrease of the U-value, and the decrease is more significant for low k_{pa}'s. For k_{pa} = 1 W/m-K, the h change from 0.3 mm to 1.5 mm results in the U-value decrease from 0.430 W/m^2-K to 0.308 W/m^2-K, while for k_{pa} = 50 W/m-K, the U-value changes from 0.524 W/m^2-K to 0.518 W/m^2-K with the same h change. Moreover, the U-value difference is less than 1% when the pillar conductivity (k_{pa}) is larger than 100 W/m-K.

Various geometries of pillars, depicted in Fig. 2.2c, were employed using FEM to study the effects of geometrical parameters, such as aspect ratio (l_1/l_2), contact surface area (A), and pillar volume (V). To examine the effect of the contact surface geometry, different aspect ratios (l_1/l_2 = 1.25, 3.2, 5, and 20) were tested in rectangular parallelepiped pillars with a constant contact surface area (A). The perimeter of contact surface increases with l_1/l_2. As presented in Fig. 2.8b, the U-value increases with l_1/l_2, suggesting smaller l_1/l_2 (or smaller perimeter) for thermal insulation, i.e., square shape has the lowest U. The l_1/l_2 dependence of U value is more significant for a higher k_{pa}, and similarly, a larger l_1/l_2 leads to a larger k_{pa} dependence (especially at lower values of k_{pa}).

Using the hollow rectangular parallelepiped pillar in Fig. 2.2c, the influence of pillar volume was studied in Fig. 2.9, excluding the contact surface area and shape. For the volume reduction of 10%, 20%, 30% and 40% by the hollow space, the U-value of the VIG quarter unit-cell model was calculated by FEM simulations with k_{pa} = 1- 999 W/m-K. As

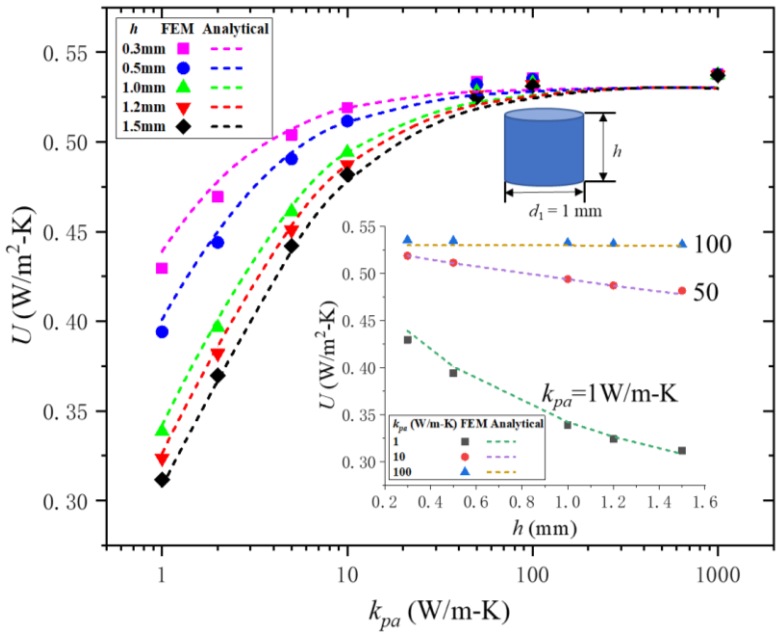

(a)

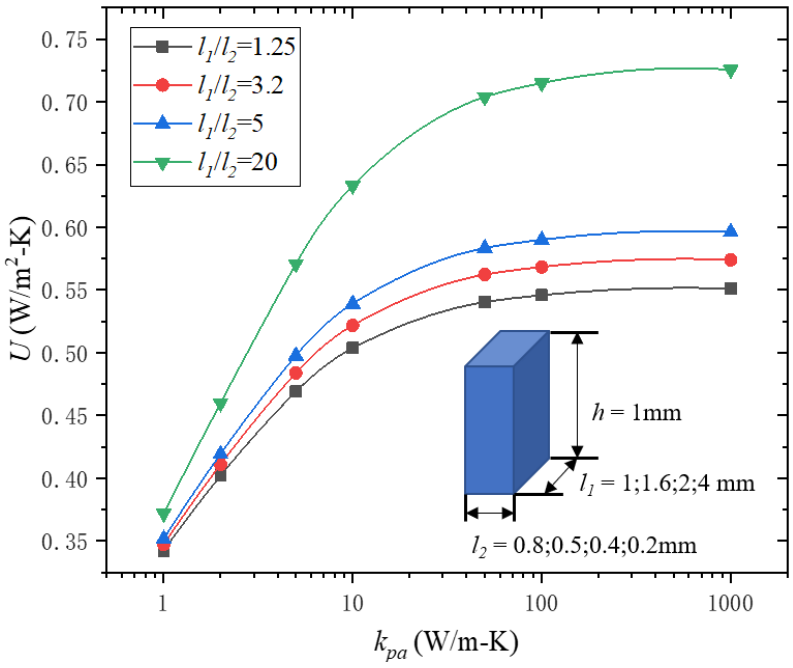

(b)

Figure 2.8. (a) *U*-value with respect to k_{pa} with different heights of cylindrical pillar (h = 0.3, 0.5, 1.0, 1.2, and 1.5 mm), and (b) that with different aspect ratios (l_1/l_2 = 1.25, 3.2, 5, and 20) of rectangular parallelepiped pillar with a fixed contact area ($A = l_1 l_2$ = 0.8 mm^2).

shown in Fig. 2.9, the *U*-value reduction due to the volume reduction is not noticeable, especially when k_{pa} is large. With the maximum volume reduction of 40%, the reduction in heat loss is 2% with k_{pa} = 50 W/m-K, and even with the lowest k_{pa} in this research, the reduction is only 15%. Considering this insignificant effectiveness for the thermal insulation and the possible harm in mechanical performance, the volume reduction by adding hollow space is not recommended.

Pillar Placement and Arrangement

Change of the pillar orientation from vertical to horizontal direction (where the axial direction is parallel to the glass panes) is expected to effectively lower the pillar conductance, by reducing the contact surface area. We calculated the overall *U*-value with respect to the pillar conductivity k_{pa} (1 – 999 W/m-K) using FEM with different cylindrical pillars as shown in Fig. 2.10. The reduction in *U*-value with length of the horizontal cylindrical pillar is larger when the pillar conductivity is larger. For a cylindrical pillar with the diameter of D = 1 mm and axial length of l = 1 mm, the horizontal placement decreases the *U*-value by 32.8% (for k_{pa} = 999 W/m-K) and 26.4% (for k_{pa} = 1 W/m-K), compared to its vertical counterpart with the same geometry. Even with a longer pillar or a larger volume, horizontal pillars lead to lower *U*-values than shorter vertical pillars. With three times larger volume or axial length (l = 3 mm), the VIG with horizontal cylindrical pillars has *U*-values similar to that with vertical pillars with the height (axial length) of 1 mm.

As expressed in Eq. (6), the spacing between the pillars is an important parameter to determine the pillar conductance, and its effect on the *U*-value was evaluated for different pillar heights (h). With an increase in the pillar spacing (λ), a smaller number of

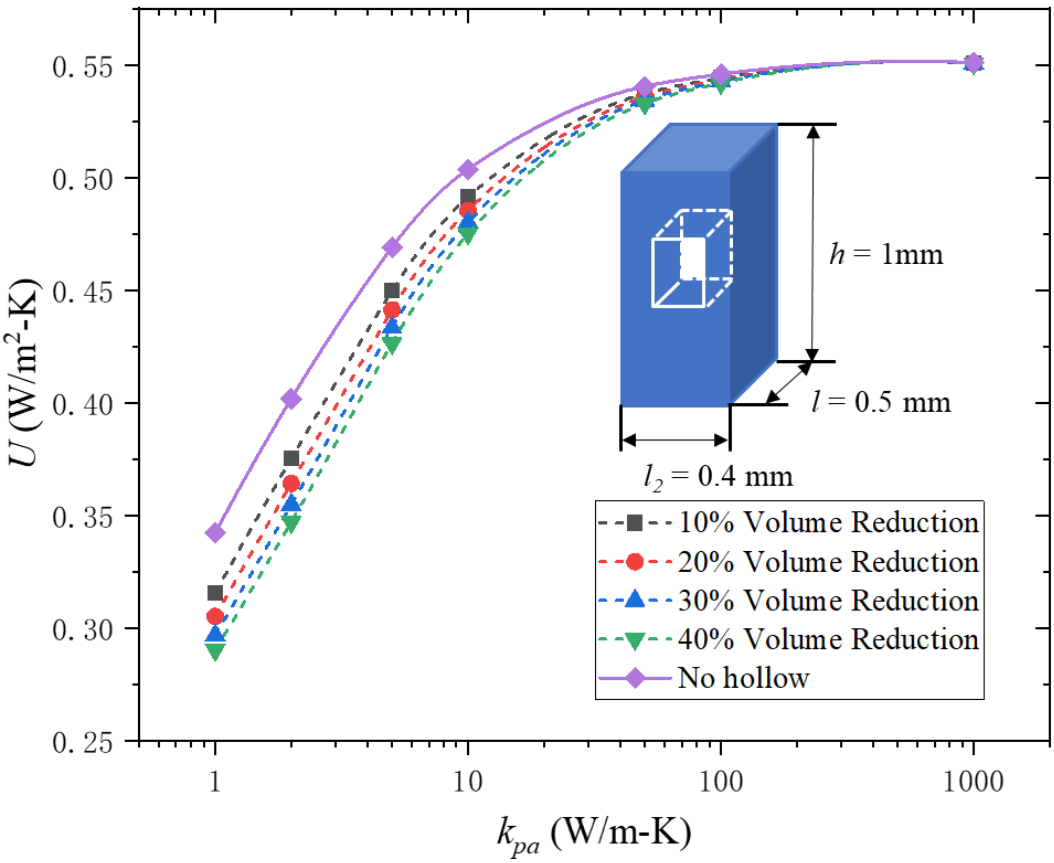

Figure 2.9. *U*-value with respect to the pillar thermal conductivity (k_{pa}) of VIG with hollow rectangular parallelepiped pillars with different volume reductions.

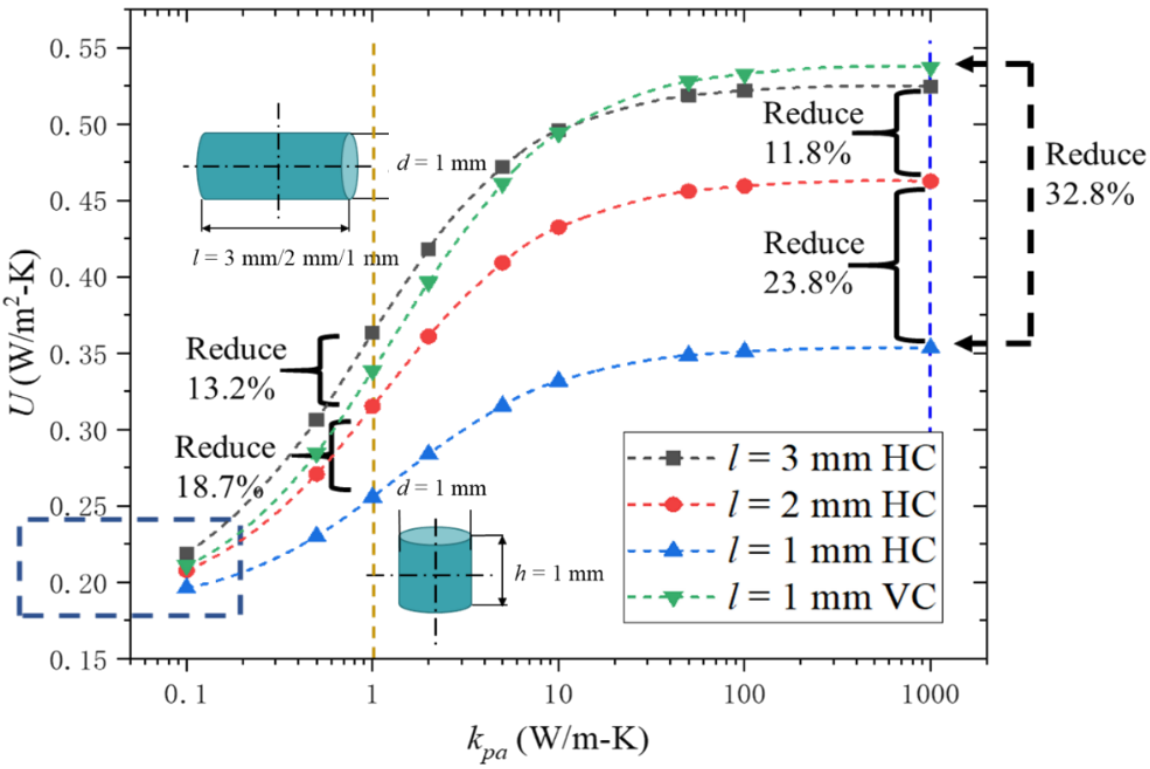

Figure 2.10. Variation of *U*-value for horizontal cylindrical (HC) pillars and vertical cylindrical (VC) pillars with respect to the pillar thermal conductivity (k_{pa}).

pillar conduction channels are available in VIG, which decreases the *U*-value. However, as shown in Fig. 2.11a and Fig. 2.11b, the larger the λ, the smaller is the decrease in *U*-value obtained by increasing λ. For example, beyond 50 mm, increase in the pillar spacing by 10 mm results in only 3% decrease in *U*-value, while nearly 40% reduction of *U*-value was observed between 15 mm spacing to 25 mm spacing. Additionally, the effect of pillar height on *U*-value becomes smaller with a larger pillar spacing. Since the pillars serve to separate the glass panes, a smaller spacing between the pillars is beneficial for structural integrity, while a larger spacing lead to lower *U*-value, and therefore choosing the appropriate spacing requires balancing both considerations.

Conductance Model Development for Rectangular Pillars

The expression for conductance given by Eq. (6) for cylindrical pillars from Collins and Fischer-Cripps[38, 39] was used as a starting point to develop a similar expression for other pillar shapes. Assuming the same values for pillar height and spacing, and applying the expression to pillars with rectangular contact area, the key parameters to be replaced are the characteristic length values '*r*' and 'πr' in the equation. Substituting *L* and L_2 in place of '*r*' and 'πr' gives the new equation:

$$C_{pa} = \frac{2k_{glass}L}{\lambda^2\left(1+\frac{2k_{glass}h}{k_{pa}L_2}\right)}. \quad (7)$$

For the case with a large value of k_{pa}, the factor $\left(1+\frac{2k_{glass}h}{k_{pa}L_2}\right)$ will be close to the unity, and Eq. (7) can be approximated as $C_{pa} = 2k_{glass}L/\lambda^2$. To verify this assumption, C_{pa} was calculated for different values of k_{pa} and different length-to-width ratios of pillars with the shape of a rectangular parallelepiped, as shown in Fig. 10a. It is observed from Fig. 2.12a that when k_{pa} is greater than 100 W/m-K, the conductance of the pillar array becomes

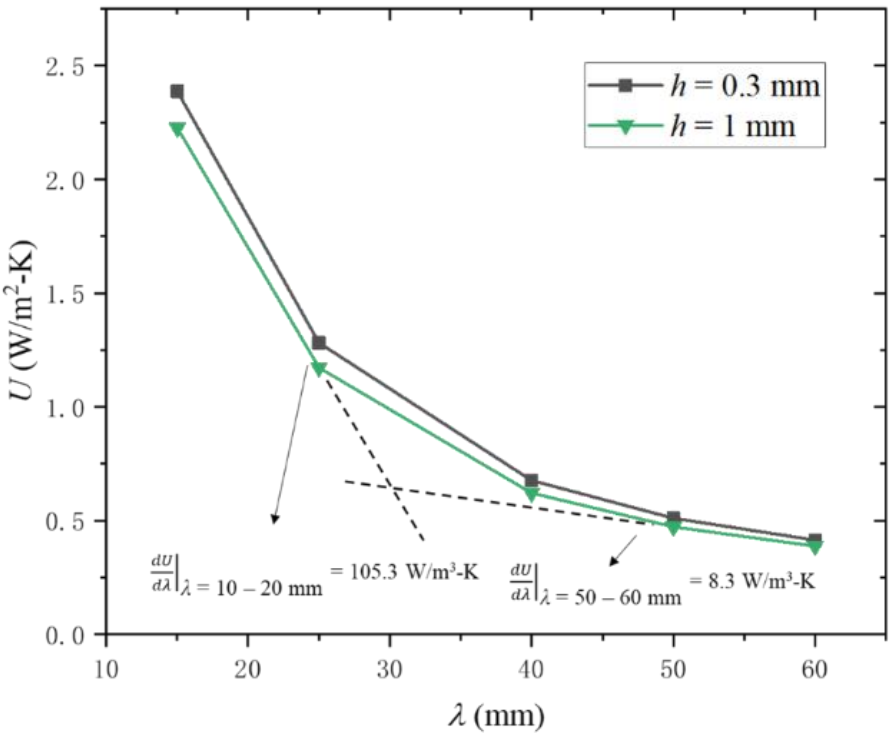

(a)

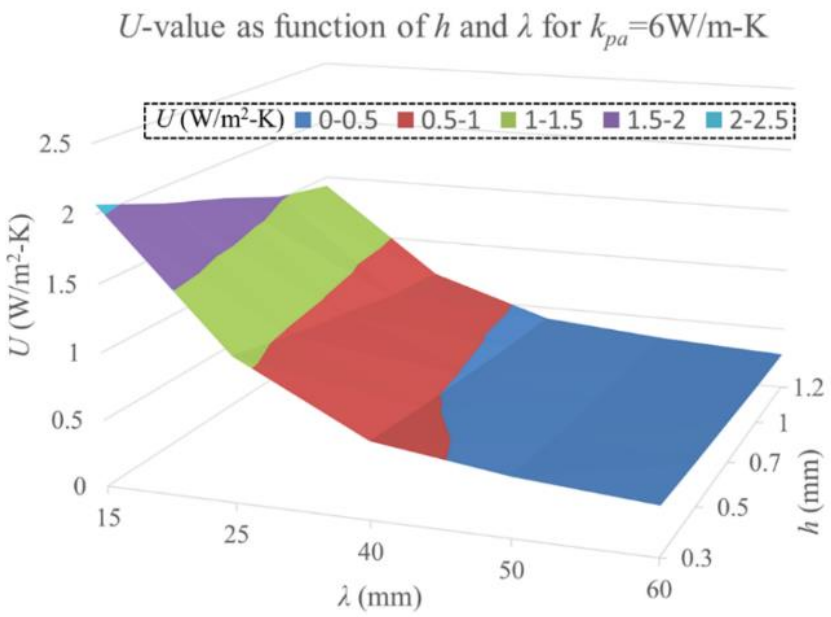

(b)

Figure 2.11. (a) 2-D plot of *U*-value for two different pillar heights and different pillar spacings with k_{pa} = 6 W/m-K; $dU/d\lambda$ is the slope value of *U*-value with respect to pillar spacing. (b) 3-D plot of *U*-value for different pillar heights and different pillar spacings with k_{pa} = 6 W/m-K.

almost constant. The dependence of C_{pa} on the pillar conductivity becomes negligible at large values of k_{pa}.

Based on this assumption, an almost linear relation was observed between the relative length and the ratio of the long side to short side of the pillar-glass contact area (Fig. 2.12b), from which we made a second assumption that the effective length $L = \beta(l_1/l_2)+B$, where β is assumed to be related to the contact area A, and B is the constant part in this formula. To verify this assumption, and to find out the expressions for β and B, we computed the VIG pillar conductance assuming different pillar-glass contact areas, with k_{pa} = 999W/m-K, as shown in Fig. 2.12c.

We found a linear relation between β and $A^{0.5}$, and between B and $A^{0.5}$, where A is the value of contact area between the pillar and the glass pane. An expression for the effective length L for the rectangular parallelepiped pillar is given by

$$L = 0.0151A^{0.5}\left(\frac{l_1}{l_2}\right) + (0.5A^{0.5} + 0.0662). \quad (8)$$

The conductance of a pillar array with large k_{pa} could be rewritten as

$$C_{pa} = 2k_{glass}[0.0151A^{0.5}\left(\frac{l_1}{l_2}\right) + (0.5A^{0.5} + 0.0662)]/\lambda^2. \quad (9)$$

The comparison between equation results and FEM results has been shown in Fig. 2.12d, this equation can be used in the situations where the VIG contains rectangular parallelepiped pillars with k_{pa} larger than 100 W/m-K and pillar heights smaller than the thickness of the glass pane, with the error being smaller than 5%. However, for cases where k_{pa} is smaller than 100 W/m-K, the equation needs further development.

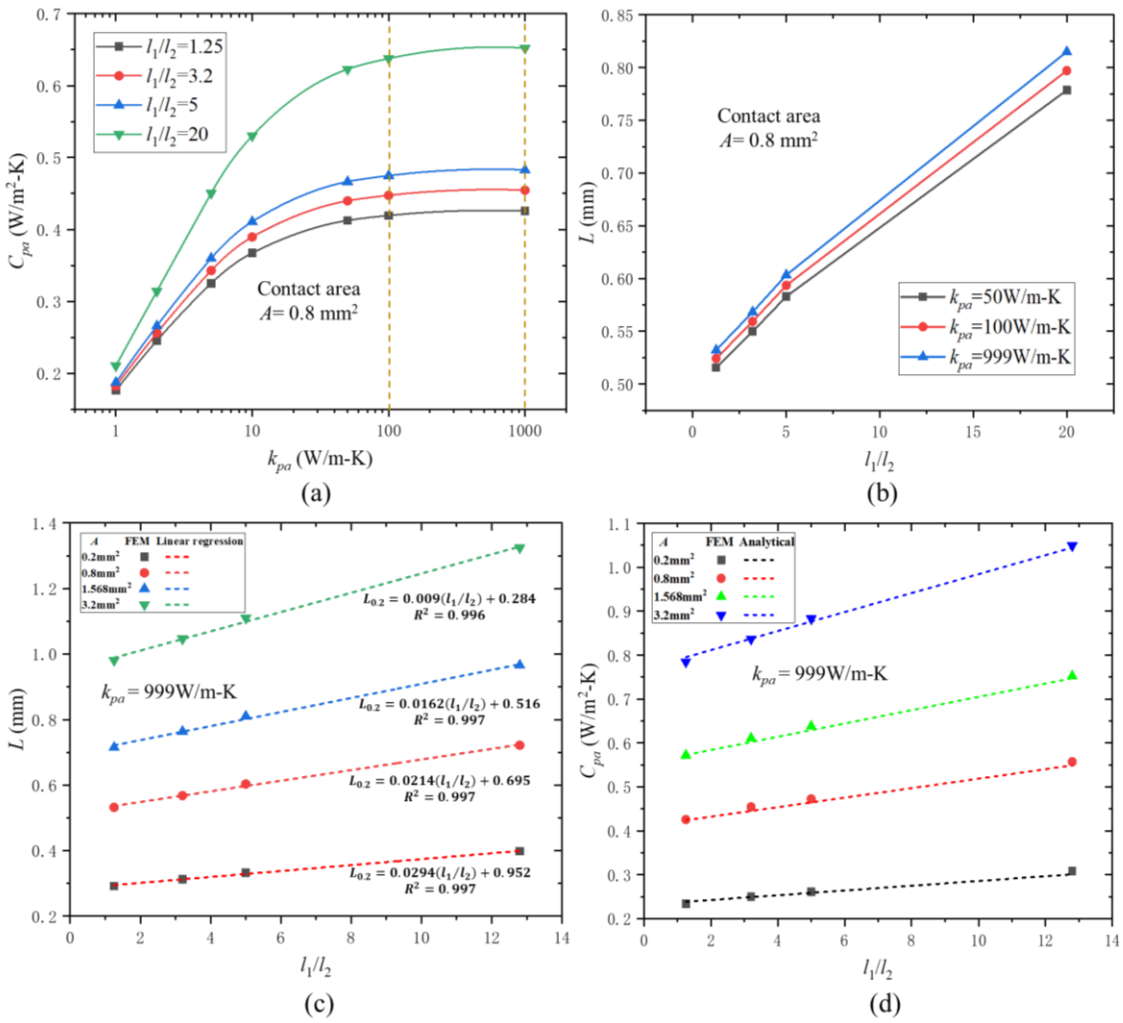

Figure 2.12. Equation development for the rectangular parallelepiped pillar. (a) pillar thermal conductance vs. pillar thermal conductivities for different ratios of l_1/l_2. (b) effective length L vs. different ratio of l_1/l_2 for different k_{pa}. (c) linear regression and R value for L vs. l_1/l_2 for different contact areas A, where each case has k_{pa} =999 W/m-K. (d) comparison between C_{pa} results with k_{pa} =999 W/m-K from FEM and C_{pa} results from Eq. (9).

2.4 Conclusions

In this research, the effects of various pillar design parameters on the thermal insulation performance of the VIG were investigated using FEM simulations (ABAQUS), along with some experimental validation and analytical calculation. The results for the thermal conductance computed using the FEM model were verified against experiment and analytical calculation, and the difference was within 3%. Based on the analysis of the FEM results, lower pillar thermal conductivity k_{pa} and higher pillar height h directly reduce the heat loss, especially when k_{pa} is lower than 50 W/m-K. If VIG contains pillars with k_{pa} higher than 50 W/m-K, the effect for pillar thermal conductivity and pillar height becomes minor. Increase in pillar spacing leads to decrease in the U-value; however, this influence becomes less significant when the pillar spacing becomes larger than 50 mm. The main reason is the reduction in the number of pillars in VIG, which leads to a decrease in gap thermal conductance and overall U-value. In addition, the effect of the pillar height becomes less significant at larger pillar spacing.

In other geometry designs, the horizontal cylindrical pillar arrangement has been shown to enhance the thermal performance, resulting in more than 25% reduction in U-value compared to the vertical cylinder. Smaller pillar volume and smaller contact area (between pillar and glass pane) with a smaller perimeter brings higher thermal performance to VIG. However, the influence of the contact area is more significant than that of the pillar volume, and even under the same value of contact area, different perimeters will significantly affect the overall U-value. An expression for thermal conductance applicable to rectangular parallelepiped pillar array was developed to help better describe the thermal

performance of VIG with non-cylindrical pillars. Based on various pillar design considerations, it can be concluded that each pillar parameter has a significant effect on the thermal performance of VIG, and some of the parameters like pillar volume, pillar contact area, pillar body shape needs to be considered together when enhancing the thermal performance of VIG. Current analytical formulas for *U*-value are limited to consideration of cylindrical pillars and need to be improved to account for other pillar shapes and arrangements. In addition, the analytical expressions are derived without consideration of the edge effects that include the primary and secondary seals and the frame. Including the edge effects can cause a significant increase in the *U*-value compared to the idealized unit cell, and therefore, the analytical expressions must be used with caution when they are applied towards the design of VIG. Optimizing the VIG for better thermal performance can be achieved through the thermo-mechanical analyses based on FEM simulations as described in this thesis.

CH 3. EFFECT OF SEALING DESIGN

3.1 Introduction

Along with pillar design, the sealing design plays another significant role in controlling the thermal transfer and providing great stress resistance, in other words, it can help enhance the thermal and mechanical performance of VIG by improving its design parameters. Research has been reported that near 50% of the overall heat transfer gets through the sealing part[44], moreover, depending on its design parameters, this ratio might take even more. Therefore, we were trying to investigate the underlying correlation between VIG performance and sealing design, especially the size and materials effect, in which way we could improve the thermal and mechanical performance of VIG.

Since 1980, investigation of how sealing materials affect the performance of regular window and evacuated windows was studied by lots of research. During the research, people were focusing on choosing a material to improve both mechanical and thermal performance of VIG with experimental tests. However, the experimental method has the unavoidable limitation in the high cost and low efficiency, each test needs to prepare several different materials and fabricate many VIG samples. Another limitation is the difficulty in testing different seal geometry properties in VIG sample, which requires to redesign the sample each time.

To solve these limitations, computational methods were applied to accompany the experiment, which can easily change the material & geometry properties and help to save the test time for more simulations. Since the 2000s, researchers begin to study the sealing effect with computational methods[45]. For example, by investigating the effect of seal size

with FEM, the research found that reducing the width of seal could bring the thermal transfer reduction around 20%[25]; alloy-seal was tested in both experiment and FEM to determine its advantage and disadvantage in sealing application[46]; effect of different seal layers mixed metal wire on the VIG performance was investigated with experiment and computational method[47].

In this chapter, we investigated the effects of various sealing parameters on the mechanical performance and thermal insulation performance of VIG, using 3D FEM coupled with experimental tests. The performance of two different types of sealing materials (flexible material and sintered glass frits) were tested and compared in our experiment. Based on this analysis, we evaluated the significance of each sealing design parameter in VIG, a detailed test result and related suggestions were provided.

3.2 Methodology

3.2.1 System Configuration of Computational Modeling

FEM simulations by ABAQUS were applied in this chapter to determine how sealing design affect the thermal and mechanical performance of VIG product. The modeling configuration has a similar design to what we used in chapter 2 (Fig. 2.1), however, to accurately investigate the sealing effect, the frame was not included, which might affect the result observation of seal effect. The configuration of the new model in this chapter was shown in Fig. 3.1.

The modeled VIG was assumed to have the top and bottom glass panes facing the outdoor and indoor environment, respectively. Both glass panes had a dimension of (1,000 × 1,000 × 3) mm^3, and a low-emittance coating with an emissivity of 0.018 was applied to

the inner surface of the top glass. The model assumed 0.133 N/m^2 (or 10^{-3} Torr) for the vacuum pressure (P_{vac}) in the gap, which is close to that used in conventional VIG products. As a benchmark or baseline condition for the study of pillar effects, cylindrical pillars with height (h) of 1 mm and radius (r) of 0.5 mm were placed in the gap and arranged in a square array with 50-mm pillar spacing (λ). A primary seal with a thickness of 1.4 mm and width of 5 mm and a secondary seal with a thickness of 1 mm and width of 7 mm were set to adhere to each other at the edge of the glass panes. Material properties for the employed FEM model are summarized in Table 1.

Because of the symmetry of the modeled window, a quarter section of the full window (500mm × 500 mm) was used in this sealing test work, which includes all the based components, the based physical properties of VIG components were shown in Table 1, and the detail of sealing was shown below (Fig. 3.2), the complex sealing design has a primary seal in the inner side and a secondary seal near it, to be specific, the primary seal contact with the vacuum gap while the secondary seal contact with the outside air. Two sealings adhesive each other and perfectly tied to the top and bottom glass panes, which is to guarantee no leaking of vacuum inside the gap.

Thermal properties and mechanical properties were changeable in our FEM simulations, the later section would show the examination of the sealing thermal conductivity (k_{seal}) ranging from 0.1 to 10 W/m-K, the heat flux distribution, and the stress distribution, etc.

All the FEM simulations for thermal and mechanical analysis were conducted using the commercial FEM program ABAQUS.

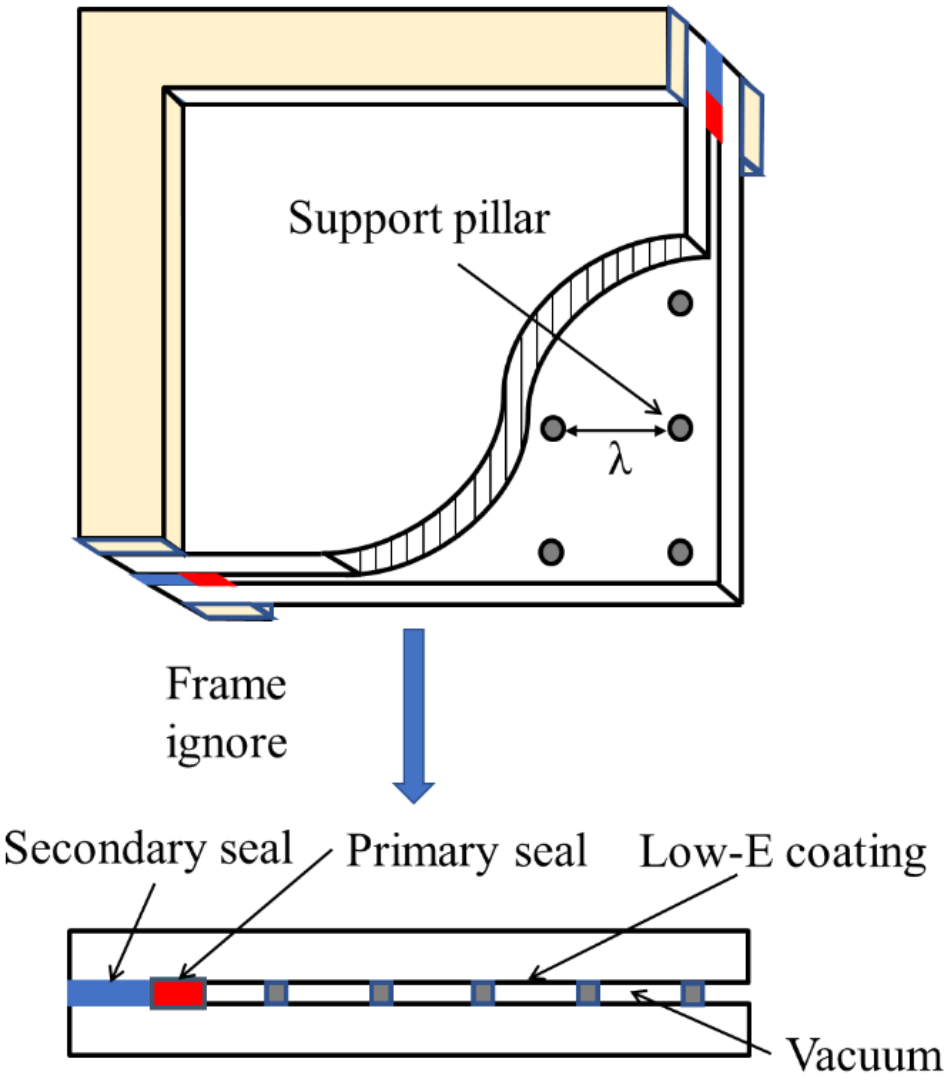

Figure 3.1. A quarter VIG model including all the details of the peripheral region without frame.

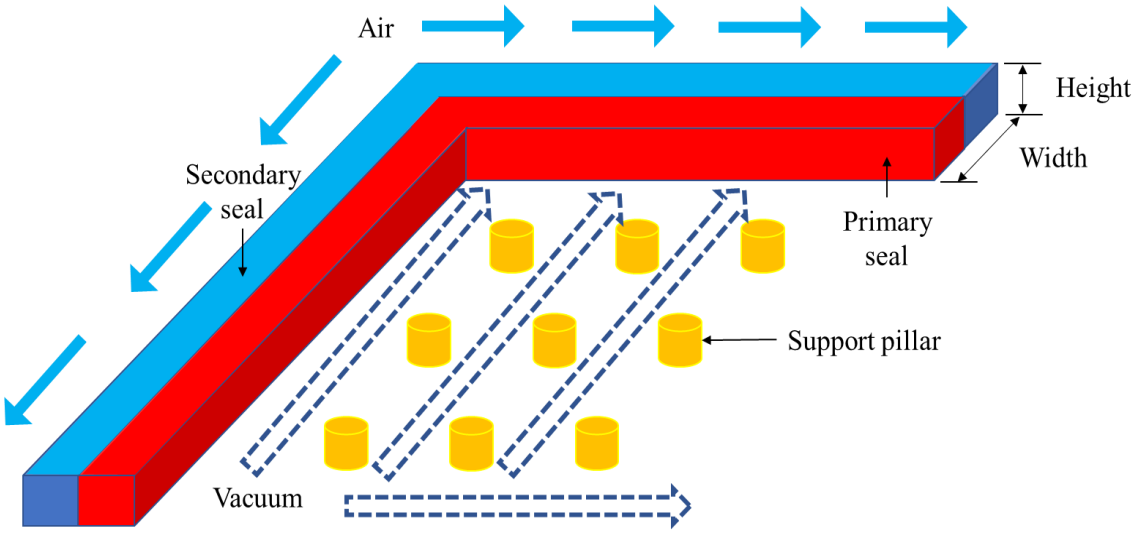

Figure 3.2. A quarter of the detailed system about seal design, the red seal and blue seal represent the primary seal and secondary seal in this system, respectively. The inside of the gap near the primary seal is filled with the vacuum and support pillars, while the outside of the gap is the air near the secondary seal.

3.2.2 Experiment

Considering the mechanical performance and product reliability of VIG, the experiment system includes airtightness tests, shear stress test, etc. to investigate the mechanical performance and its reliability. Water container and freezer were applied in the airtightness test, while tensile machine was used for the shear stress test as shown in Fig. 3.3.

To make a comparison between different VIG designs and guarantee the accuracy in this test, the geometry details of our test sample had differences between different tests. In Fig.3.4, 3” x 3” to 6” x 6” VIG with 0.5-inch width sealing had been made to satisfy each experimental test. For the shear stress test, to guarantee its efficiency in fabrication and accuracy in the test, a smaller and simple sample with two glass panes and single line of seal was applied besides the regular sample used before.

To satisfy this comparison process and investigate a new type of sealing, our experiment system has two different types of materials employed to make the seal, one is the seal with flexible materials made which is commonly used in current window product, another is the sintered glass frits, which has significantly different properties and fabricate process than flexible seal.

For flexible seal, 24-48 hours curing to become a rubber at room temperature is necessary after directly adhesive to two different glass panes, while for glass frits, a 3D printing and high temperature sintered is necessary, our lab was using the 3D printer and laser system to fabricate it to a laser seal (Fig. 3.4). Due to these two different processes, the properties of these two products have obvious difference, the flexible seal still

(a)

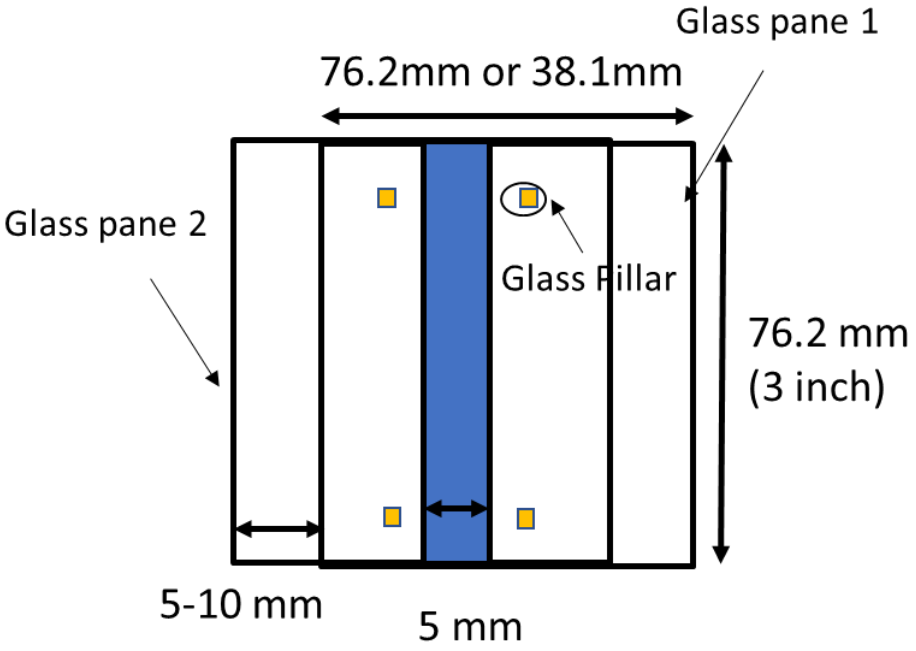

(b)

Figure 3.3. (a) Tensile machine Model QC-TECH B5000 system with the sample inside (b) Configuration detail of the model to test shear stress of the seal. The top glass pane and bottom glass pane have a 5-10 mm dislocation, seal (blue line in the figure) is in the overlap place of two glass panes. 4 pillars are using to make sure the gap height is consistent.

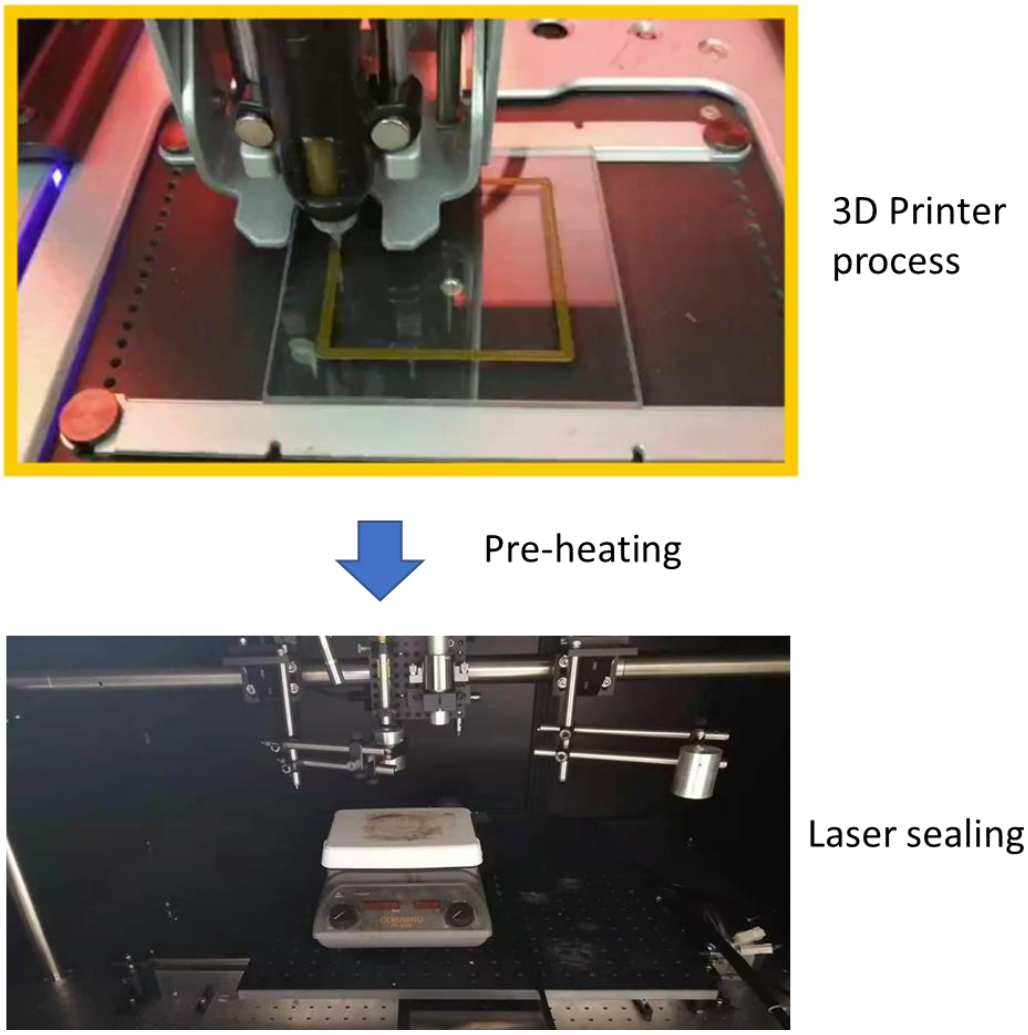

Figure 3.4. Glass frit seal fabricating process including 3D printer and laser seal process system, after 3D printing, glass sample with glass frits seal would be set on the white plate and be heated and sintered by using laser on the top.

performed great elasticity (lower Young's modulus) while the ink seal shows high Young's modulus. To determine the mechanical performance of these two seals, shear stress test with tensile machine was applied.

Additionally, to improve the airtightness of flexible seal, glass power (diameter < 0.2mm) was applied in the sealing process. To determine the detail influence of this process, different ratio of glass power mixed flexible seal was test and presented in the later part.

Several VIG samples with flexible seal and laser seal have been fabricated, each sample was applied in different experiment tests. In Fig. 3.5. four different seal-glass samples were presented.

3.3 Results and Discussion

3.3.1 Thermal Effect of Sealing Parameters

Thermal conductivity effect

In FEM simulations, the thermal conductivity of seal was changed to determine the correlation between the overall *U*-value of VIG and itself, 4 different pillar thermal conductivity values were applied to see the tendency in 3 different sealing design parameters. From Fig. 3.6, the results indicated that, with the increment of k_{seal}, the *U*-value increased, however, this tendency becomes slow and flat after k_{seal} >1W/m-K. On the other hand, with different k_{pa}, the tendency of k_{seal} and *U*-value stay consistent, while the value increased with the increased k_{pa}, this increasing jumps fast from k_{pa} = 1 W/m-K to k_{pa} = 16 W/m-K and becomes smaller and smaller after k_{pa} > 16 W/m-K.

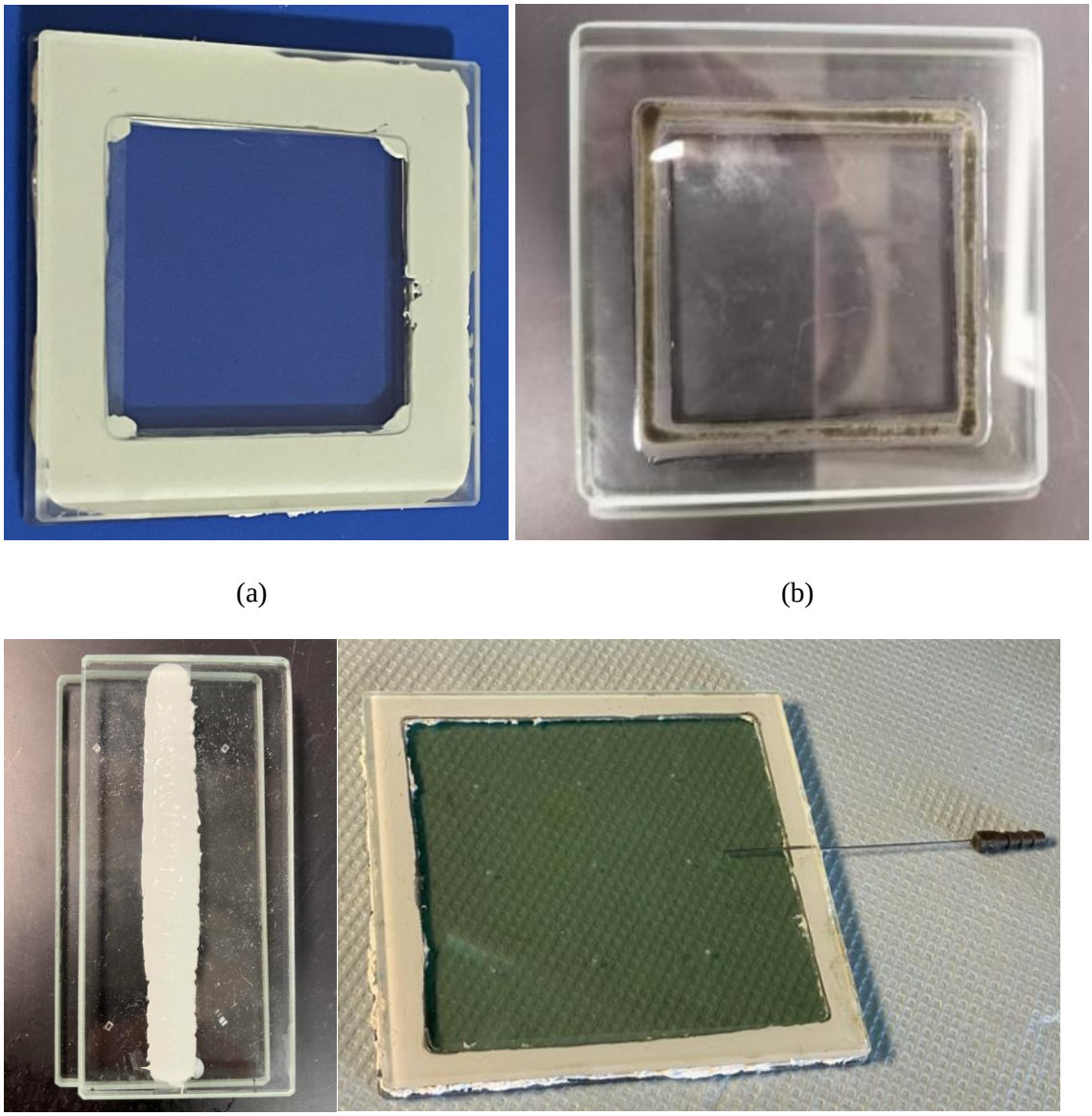

(a) (b)

(c) (d)

Figure 3.5. Four different samples in experimental test (a) 3” × 3” glass with flexible seal, (b) 3” × 3” glass with laser seal, (c) 1.5” × 3” glass with single line flexible seal, mainly used in stress test, (d) 6” × 6” glass with flexible seal.

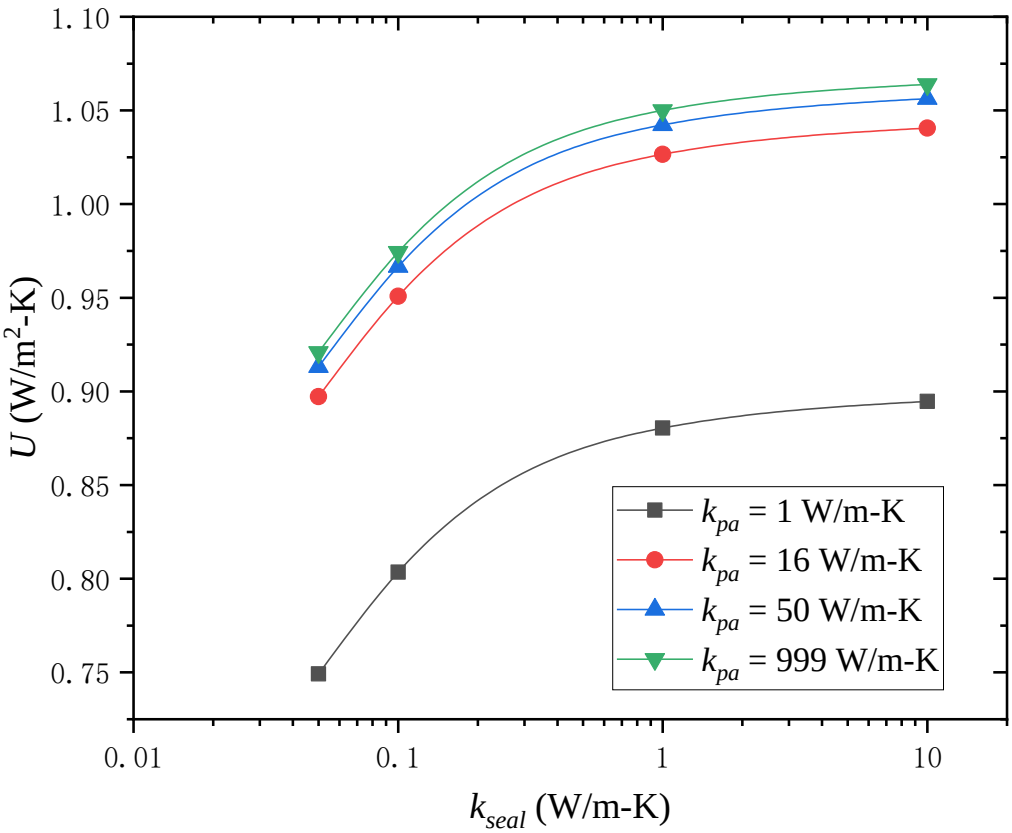

Figure 3.6. *U*-value to different thermal conductivities of seal and pillar, k_{seal} is from 0.05 W/m-K to 10 W/m-K while the k_{pa} is from 1 W/m-K to 999 W/m-K.

It can be deducted from the results that the thermal influence from seal becomes slight and could be ignored after k_{seal} larger than 1 W/m-K, if consider using the regular thermal conductivity of flexible materials, most of the flexible materials have thermal conductivity under 1 W/m-K[48], therefore, any different type of them might bring significant effect to the overall VIG thermal performance.

Heat flux distribution

To determine the detail of this seal thermal effect, the heat flux (HFL) distribution through the center of VIG was presented. We chose two different paths near the center of VIG, the path 1 is the center line on the top surface of the outdoor glass pane which goes through the *xy* location of support pillars, the path 2 is the line that has λ/2 distance to the path 1 which makes it does not go through and *xy* coordinate of support pillars. The detail of the two paths was shown in Fig. 3.7(a), and the results of heat flux distribution were presented in Fig. 3.7(b).

From the results, the heat flux through path 1 and path 2 performed different performance in the distribution plot, the path 1 which include the pillar effect has a peak level heat flux value per pillar, while the distribution in path 2 only has a slight pillar effect. The heat flux has a high value near the seal position and pillar position, the distribution after 100 mm becomes a stable wave, which indicated that the affected area of seal is limited. Therefore, to accurately investigate how thermal conductivity of seal and pillar affect the heat flux distribution, we chose 0-100 mm of path 1 and path 2 as the new test range and applied the case of different k_{pa} and k_{seal}. The results were shown in Fig. 3.8.

We calculated the heat flux distribution with respect to the pillar thermal conductivity k_{pa} (1-999 W/m-K) in part of path 1 (0-100 mm) and path 2 (0-100 mm), the thermal conductivity of seal was fixed at k_{seal} = 1 W/m-K. From the details that were shown in fig. 3.8 (a) and (b), the heat flux around the seal has a high value and generally decreases after the distance is larger than 12.5 mm which is the side of the seal. The pillar thermal conductivity is going to affect the distribution of heat flux after distance is larger than 30 mm which is 140% larger than the width of seal. However, this effect becomes stable after k_{pa} larger than 16W/m-K, and the effect only brings a slight difference if the distribution does not go through path 1.

From the results above, the heat flux through path 1 and path 2 performed different performance in the distribution plot, the path 1 which include the pillar effect has a peak level heat flux value per pillar, while the distribution in path 2 only has a slight pillar effect. The heat flux has a high value near the seal position and pillar position, the distribution after 100 mm becomes a stable wave, which indicated that the affected area of seal is limited. Therefore, to accurately investigate how thermal conductivity of seal and pillar affect the heat flux distribution, we chose 0-100 mm of path 1 and path 2 as the new test range and applied the case of different k_{pa} and k_{seal}. The results were shown in Fig. 3.8.

We calculated the heat flux distribution with respect to the pillar thermal conductivity k_{pa} (1-999 W/m-K) in part of path 1 (0-100 mm) and path 2 (0-100 mm), the thermal conductivity of seal was fixed at k_{seal} = 1 W/m-K. From the details that were shown in fig. 3.8 (a) and (b), the heat flux around the seal has a high value and generally decreases after the distance is larger than 12.5 mm which is the side of the seal. The pillar thermal

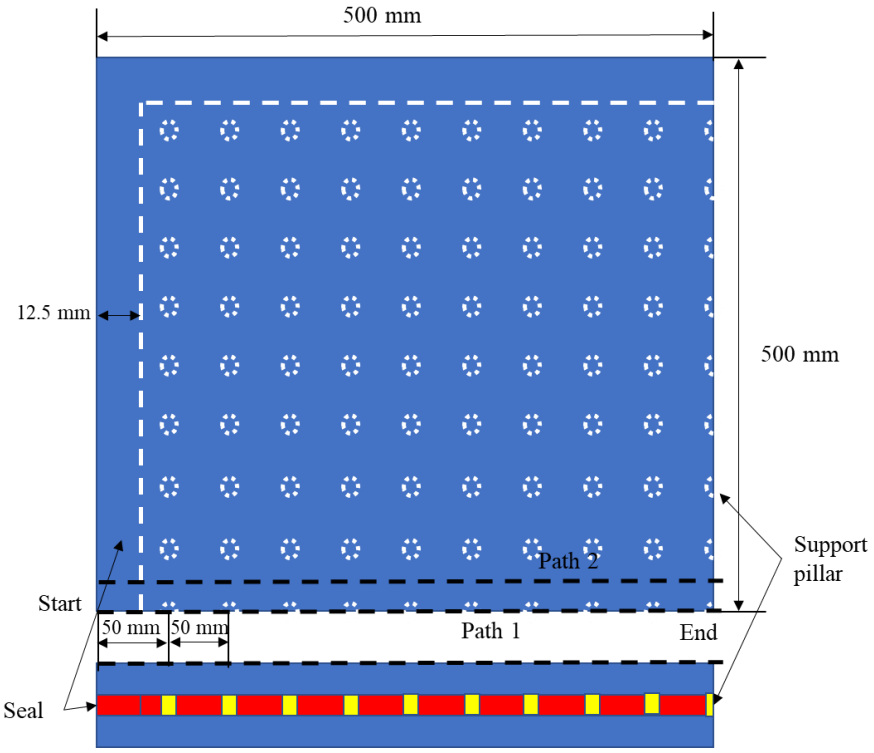

(a)

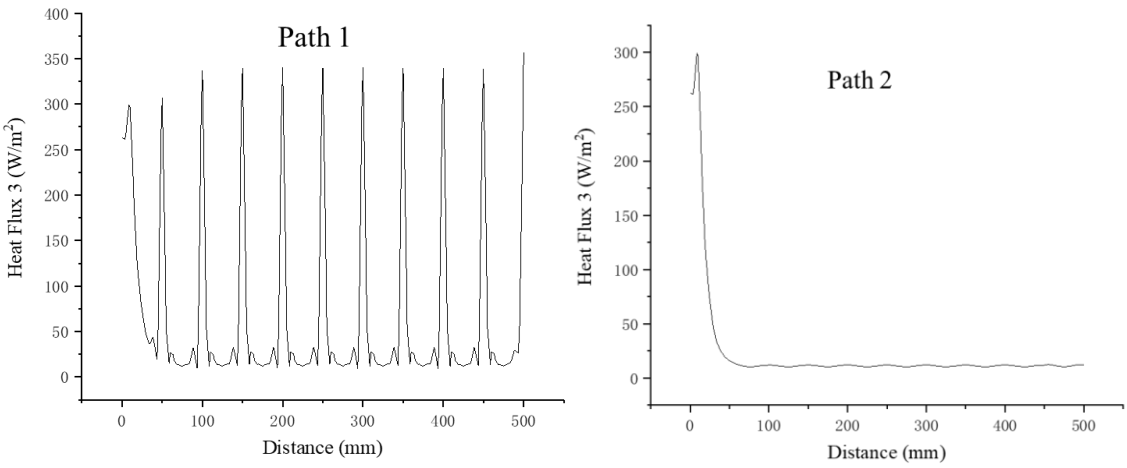

(b)

Figure 3.7. (a) Detail of quarter of VIG FEM model with two different paths, path 1 is in the center of VIG, path 2 has a 25 mm (λ/2) distance to the path 1. (b) Heat flux distribution through two different paths with k_{seal} = 1W/m-K and k_{pa} = 16 W/m-K.

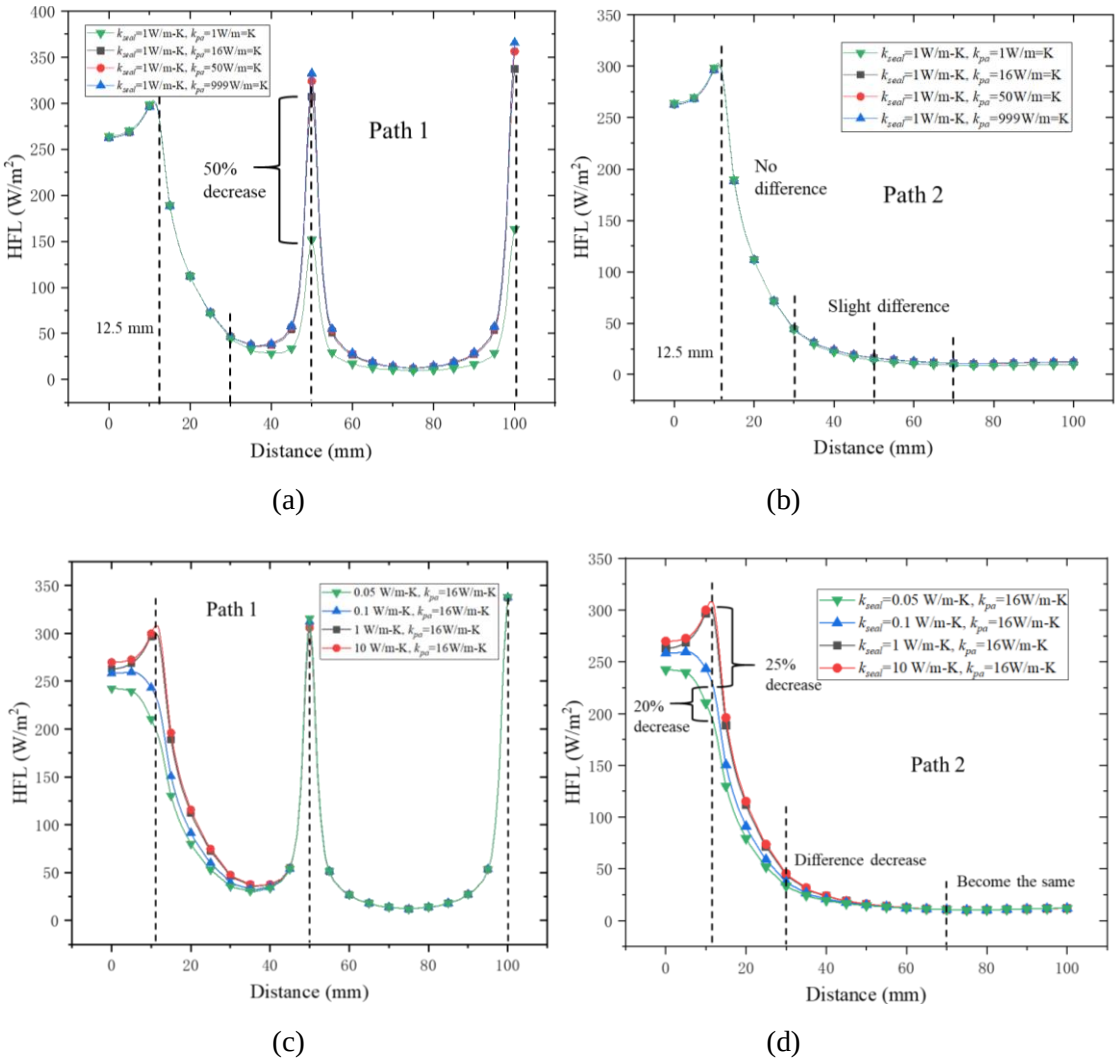

Figure 3.8. Heat flux distribution through two different paths with different k_{seal} and k_p: (a) heat flux distribution through path 1 with k_{seal} =1 W/m-K and k_p = 1-999W/m-K; (b) heat flux distribution through path 2 with k_{seal} =1 W/m-K and k_p = 1-999W/m-K; (c) heat flux distribution through path 1 with k_{seal} =0.05-10 W/m-K and k_p = 16 W/m-K; (d) heat flux distribution through path 2 with k_{seal} =0.05-10 W/m-K and k_p = 16 W/m-K.

conductivity is going to affect the distribution of heat flux after distance is larger than 30 mm which is 140% larger than the width of seal. However, this effect becomes stable after k_{pa} larger than 16W/m-K, and the effect only brings a slight difference if the distribution does not go through path 1.

In Fig. 3.8(c) and (d), we calculated the heat flux distribution with respect to the different seal conductivity k_{seal} (0.05-10 W/m-K), the pillar conductivity is equal to 16 W/m-K. The changing of seal effect does not make significant influence beyond the field around the pillar. On the other hand, when distance larger than 30 mm (140% of seal width) the heat flux in different k_{seal} cases only have a slight difference, and this difference would disappear after distance larger than 70 mm. The maximum heat flux difference is in the side of seal, which has a 25% decrease from k_{seal} = 1 W/m-K to k_{seal} = 0.1 W/m-K and a 20% decrease from k_{seal} = 0.1 W/m-K to k_{seal} = 0.05 W/m-K.

3.3.2 Mechanical Effect of Sealing Parameters

In mechanical effect test, several different samples based on two types of sealing were applied. Besides the pure flexible seal and pure glass frit, the flexible seal with different ratios of glass powder mixed (0%, 10%, 20%, 30%) were tested in our experiment to investigate the improvement of airtightness and shear stress for flexible seal.

The mixed results were shown in Fig. 3.9. flex materials mixed with different ratios of glass power present different performances. With the increase of ratio, the flexible seal is more likely to lose its fluidity before curing, once the ratio is larger than 40%, most of the fluidity would lose, therefore, we chose the ratio below 40% in our sample making and experimental test.

Airtightness test

A 9 mm deep water container was employed in this airtightness test, samples with different materials and different sizes were horizontally set in the bottom of the container for more than 48 hours like below.

Sample of glass with pure flexible seal and laser seal showed great performance in the airtightness test, no water gets into the gap of the sample after 48 hours. The sample of glass with flexible seal with 10-30% ratio of glass power mixed also brought a good performance in this test. All these samples performed great performance to pass the airtightness test with sizes of 3" × 3" and 6" × 6", which not only provide a guarantee to further test in our research but also indicated that the size might not affect too much for the seal airtightness. To validify this conclusion, although we did not make it in current work, further work about the 1 mm × 1 mm VIG sample is necessary.

Since each sample proved its ability in preventing vacuum leaking, the next step for sample test is about their performance in stress test (Fig. 3.11).

Stress and displacement in different directions.

Because of the vacuum inside the gap of VIG, the atmosphere around the outside of VIG could bring huge stress and possible damage to VIG products. The result of displacement and stress distribution from FEM simulations was presented in fig. 2.5, along with the pillar, seal afford a huge part of stress, especially the shear stress. Therefore, a shear stress test was the main task in this part. To investigate the performance of each seal to afford shear stress, we first calculated the shear stress distribution with FEM simulations.

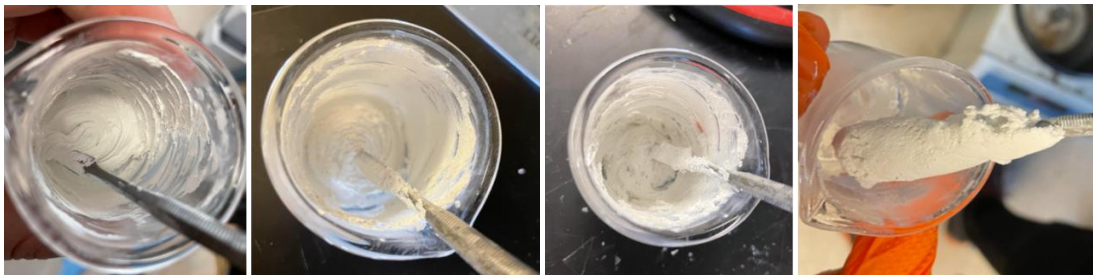

(a) (b) (c) (d)

Figure 3.9. Flexible seal mix with different volume ratios of glass powder smaller than 0.2 mm. (a) flexible seal mix with 10% glass powder; (b) flexible seal mix with 30% glass powder; (c) flexible seal mix with 40% glass powder; (d) flexible seal mix with 50% glass powder.

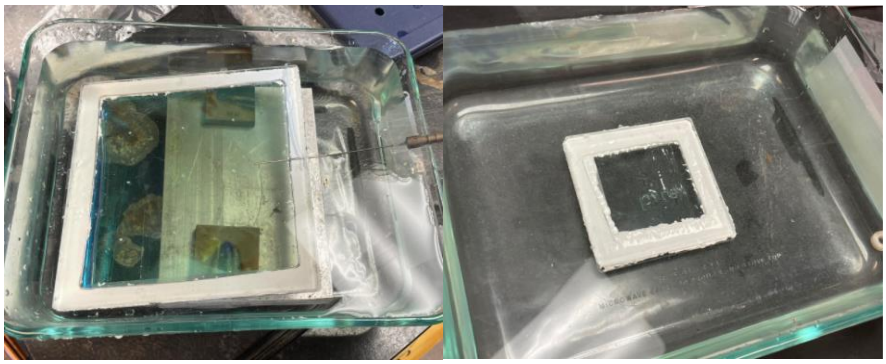

(a) (b)

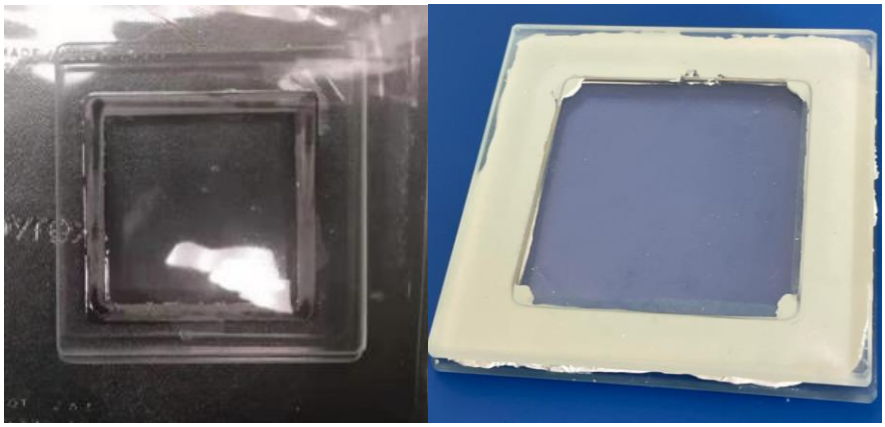

(c) (d)

Figure 3.10. Airtightness test result for four different samples: (a) 6” × 6” glass with flexible seal (b) 3” × 3” glass with flexible seal (c) 3” × 3” glass with laser seal (glass frit); (d) 3” × 3” glass with flexible seal mixed glass power.

From the results in Fig. 3.12. the increased ratio of glass power in the flexible seal results in the weaker maximum shear stress afford. When the ratio of mixed glass powder increased from 0% to 30%, the maximum shear stress τ_{max} decreased by 1.1%, however, when the ratio of glass powder increased from 30% to 35%, the τ_{max} decreased by 16.5%. It can be deduced that a high volume of glass powder might break the structure of flexible materials, which leads to a bad performance in the stress afford.

The maximum shear stress of a laser seal is around 4 MPa, which is near 4 times larger than pure flexible seal. However, the deformation resistance of laser seal is much lower than flexible seal, only 18.5% strain before breaking the glass with laser seal. While the flexible seal has around 16% strain range before the yield strength and 28% strain range before the ultimate strength. The reason should be the huge difference between their Young's modulus, which led to the different performance in this deformation resistance.

FEM simulations were used to determine the shear stress during a 1 m × 1 m working VIG system. Based on the different types of material, simulation applied the low Young's modulus group cases (20 MPa – 100 MPa) and high Young's modulus group cases (100 GPa – 150 GPa)[49]. The result of lower Young's modulus cases which is to stimulate the flexible seal has maximum shear stress from τ = 0.09 MPa – 0.42 MPa, the results were 2-10 times smaller than the maximum shear stress resistance of flexible in our experiment result, which can be deduced that the flexible is stable enough to afford the press in a 1 m × 1 m working VIG system. However, the laser-sintered glass frits had maximum shear stress τ from 9.5 MPa to 11.5 MPa, which is more than 2 times of our maximum shear stress resistance in experiment test. The reason could be conjectured as

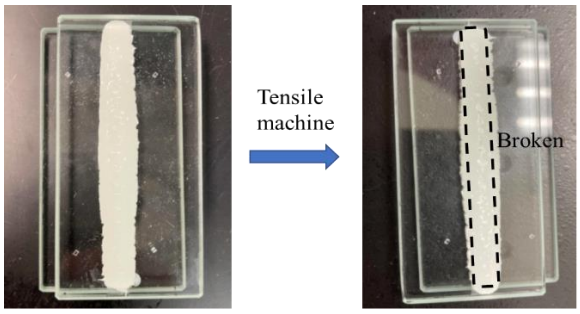

Figure 3.11. Shear stress test using tensile machine and a sample of glass with pure flexible seal.

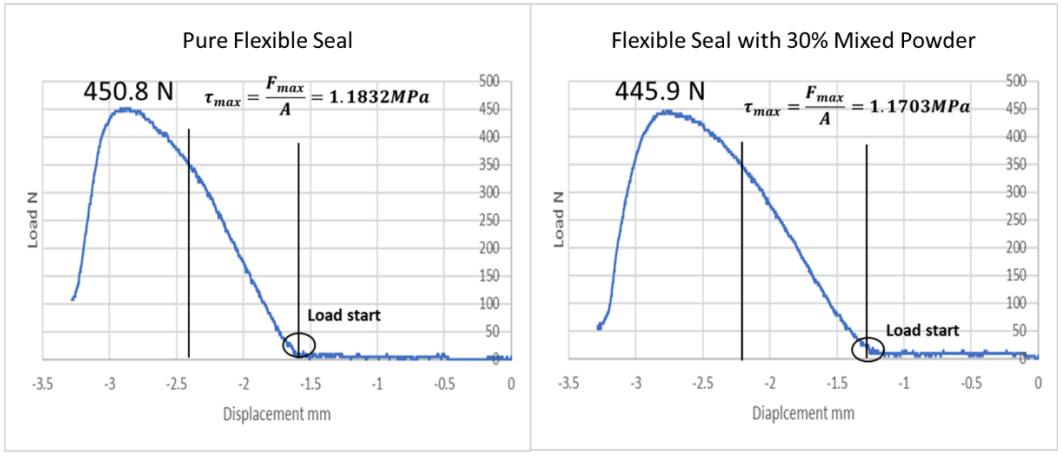

(a) (b)

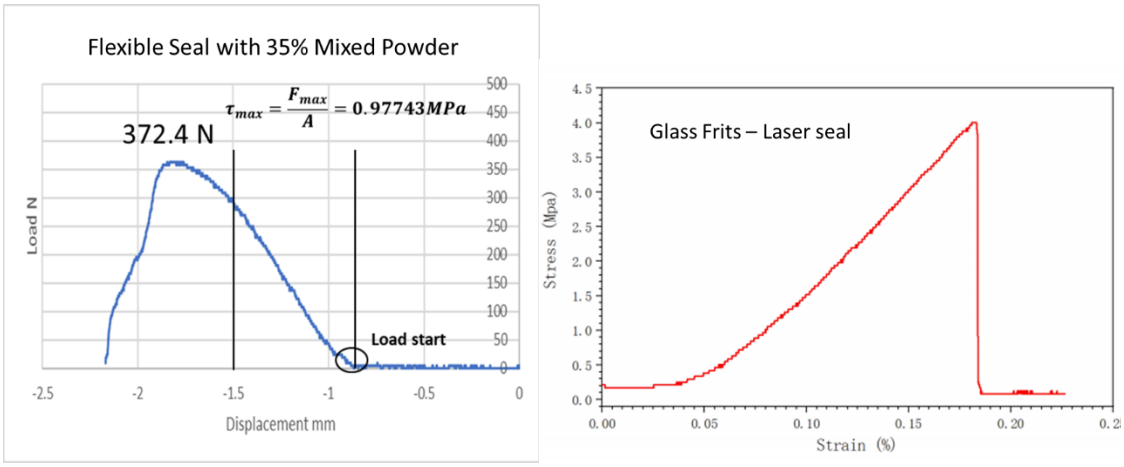

(c) (d)

Figure 3.12. Shear stress test result for glass with four different seals: (a) pure flexible seal, (b) flexible seal mixed with 30% glass powder (c) flexible seal mixed with 35% glass powder (d) glass frits.

the deficiency during the process of laser-sintered, the inhomogeneous heating and cooling may take damage to its structure. To validate this assumption, ambient thermal curing using a heating chamber system was applied instead of using laser, the results of maximum shear stress are about 20-30 MPa, which is 2-3 times larger than FEM results. Therefore, the materials of sintered glass frit have great strength to afford the press during the working VIG system, however, the laser-sintered process still needs to be improved in further work.

3.4 Conclusions

In this chapter, the effects of sealing design on the thermal and mechanical performance of VIG were investigated using FEM simulations and experimental tests. Several VIG samples were fabricated for experimental tests including airtightness test and shear stress test. The thermal performance of VIG was tested under different seal designs and pillar designs to study the details of seal effect.

Based on the analysis of FEM results, the lower seal conductivity k_{seal} can bring the lower *U*-value to VIG system, the significance of this influence depends on the range of k_{seal}, if $k_{seal} > 1$ W/m-K the influence becomes insignificant which only bring 5% difference of *U*-value from $k_{seal} = 1$ W/m-K to $k_{seal} = 10$ W/m-K. The heat flux distribution indicated the region of seal effect can extend to 140% more than the width of seal, different k_{seal} could affect the value of heat flux around the seal, especially when k_{seal} is smaller than 1 W/m-K. However, this influence becomes smaller and smaller after k_{seal} is larger than 1 W/m-K or the distance to the seal is 140% more than the width of the seal. We also employed the pillar conductivity k_{pa} as a changeable parameter, but it does not bring any significant influence on the sealing effect.

In mechanical performance tests, two different materials of seal, flexible seal and glass frits, were employed in our experimental test. Both materials have great performance in the airtightness test and shear stress test, the glass frits have great shear stress resistance than flexible while the deformation resistance is weaker than flexible. To validify how the maximum shear stress works in the working VIG, FEM simulations were applied to test the details of shear stress at the seal. The results are 2-10 times smaller than the maximum shear stress of flexible seal, which guarantees stability in the 1 m × 1 m working VIG. However, the shear stress simulation result of sintered glass frits seal is larger than our experiment, which indicated that it cannot afford the press in a 1 m × 1 m working VIG system. The reason should be in the process of laser sintering, which we need to improve during further work.

The flexible seal with different ratios of fine glass powder was tested in our experiment, with below 30% volume of glass powder mixed, it performed great performance in airtightness test and shear stress test. However, when the ratio is larger than 40%, the material would lose most of its fluidity and could not be used to adhesive the glass pane, and the maximum shear stress resistance would decrease with the increasing of ratio.

CH 4. SUMMARY AND FUTURE WORK

4.1 Summary and Impacts

In this research, I investigated the mechanical and thermal performance of vacuum insulated glass and the effects of pillar and sealing design on the performances. Through the comprehensive computational and experimental study, the correlations of various design parameters with thermal conductance and mechanical strength were identified, presenting the significance of the optimized pillar and seal design.

(1) In the investigation of pillar design, the thermal conductance that was computed using the FEM model was verified against experiment and analytical calculations, and the difference was within 4%.

Based on the analysis of the FEM results, a higher value applied in pillar height and a lower value applied in pillar thermal conductivity led to the reduction of heat loss in VIG system. This effect becomes significant if the thermal conductivity is smaller than 50 W/m-K. Increasing the pillar spacing also results in the decreasing in *U*-value, which is due to the reduced number of support pillars. However, when the pillar spacing is larger than 50 mm, this influence becomes minor and minor. If consider the correlation of both pillar height effect and pillar spacing effect, the larger pillar spacing design would bring less significance of pillar height effect.

In the shape design of pillar, the pillar arrangement, pillar volume, contact area (between pillar and glass) could bring significant effect to the overall thermal performance of VIG system. I have found out that changing the vertical cylinder pillar into the horizontal cylinder pillar could lead to a more than 25% reduction in *U*-value. The smaller pillar

volume and contact area (between pillar and glass pane) with smaller perimeter could bring higher thermal performance of VIG, however, contact area had more significant influence than pillar volume. The perimeters also affect the *U*-value of VIG system, even under the same contact area, smaller perimeters could bring a huge reduction in heat loss. An expression for thermal conductance applicable to a rectangular parallelepiped pillar array was developed to help better describe the thermal performance of VIG with non-cylindrical pillars.

(2) In the study of sealing design, FEM simulations and experimental tests were applied in our research to investigate the sealing effect on thermal and mechanical performance of VIG. During the thermal performance study, the seal thermal conductivity k_{seal} performed significant influence when $k_{seal} < 1$ W/m-K, if the k_{seal} is larger than 1 W/m-K the influence becomes insignificant. Besides, the seal could bring higher heat flux around the seal, the field could extend to the distance of 140% of seal width. The changing of pillar conductivity only has a minor effect on this heat flux distribution around the seal.

Two different materials of seal, flexible seal and sintered glass frits were examined in our experiments. The flexible seal demonstrated a good airtightness and a larger deformation resistance due to the low Young's modulus. On the other hand, sealing with sintered glass frits provides a limited shear strength although it can achieve a tight seal. Additionally, the experiment includes the flexible seal mixed with different ratios of glass powder (volume) which can increase the airtightness of seal, the results showed that with the increase of ratio, the shear stress resistance of flexible became weaker, and 30% of glass powder is recommended for the strength and compactness.

4.2 Recommendations for Future Studies

Currently, available expressions of thermal transport in pillar and seal have limitations in describing the pillar and seal which have different shapes in a low pillar thermal conductivity. The development of simple equations to calculate the thermal conductance of seal and support pillar in various conditions will be beneficial to facilitate the VIG design.

Additionally, I have already demonstrated the significant role of seal in both thermal and mechanical performance of VIG, however, the study of sealing design parameters is still insufficient. More diverse geometries of seal need to be investigated in further work, and the processing conditions of sintered glass frits can be further improved.

REFERENCES

1. *Review of Cost Effectiveness Analysis.* ENERGY STAR for Windows, Doors, and Skylights Version 6.0 Criteria Revision.

2. Benson, D., et al., *Vacuum window glazings for energy-efficient buildings*. 1990, Solar Energy Research Inst., Golden, CO (USA).

3. Grynning, S., et al., *Windows in the buildings of tomorrow: Energy losers or energy gainers?* Energy and buildings, 2013. **61**: 185-192.

4. Zoller, F., *Hollow pane of glass.* German patent, 1924. **387655**.

5. Robinson, S. and R. Collins. *Evacuated windows-theory and practice*. in *ISES solar world congress, international solar energy society, Kobe, Japan*. 1989.

6. Aggas, S.L. and V.S. Veerasamy, *Vacuum IG unit with spacer/pillar getter*. 2002, Google Patents.

7. Bao, M., et al., *Novel hybrid vacuum/triple glazing units with pressure equalisation design.* Construction and Building Materials, 2014. **73**: 645-651.

8. Collins, R.E., et al., *Vacuum glazing—a new component for insulating windows.* Building and Environment, 1995. **30**(4): 459-492.

9. Koebel, M.M., et al., *Anodic bonding of activated tin solder alloys in the liquid state: a novel large-area hermetic glass sealing method.* Solar energy materials and solar cells, 2011. **95**(11): 3001-3008.

10. Manz, H., S. Brunner, and L. Wullschleger, *Triple vacuum glazing: Heat transfer and basic mechanical design constraints.* Solar Energy, 2006. **80**(12): 1632-1642.

11. Cuce, E., C.-H. Young, and S.B. Riffat, *Thermal performance investigation of heat insulation solar glass: a comparative experimental study*. Energy and Buildings, 2015. **86**: 595-600.

12. Eames, P.C., *Vacuum glazing: Current performance and future prospects.* Vacuum, 2008. **82**(7): 717-722.

13. Griffiths, P., P. Eames, and B. Norton. *Thermal properties of evacuated glazing based on experimental solar simulation and computer based simulation modelling*. in *Int. Conference on Building Envelope Systems and Technology (ICBEST'97)*. 1997. University of Bath.

14. Clugston, D. and R. Collins, *Pump down of evacuated glazing.* Journal of Vacuum Science & Technology A: Vacuum, Surfaces, and Films, 1994. **12**(1): 241-247.

15. Griffiths, P., et al., *Fabrication of evacuated glazing at low temperature.* Solar Energy, 1998. **63**(4): 243-249.

16. Turkington, R. and R. Harris-Lowe, *Note on the design of simple indium O-ring seals.* Review of scientific instruments, 1984. **55**(5): 803-805.

17. Teeter, R. and W. Doty, *Glass Vacuum Seal to Operate at High Temperatures.*

Review of Scientific Instruments, 1966. **37**(6): 792-793.

18. Horwitz, N. and H. Bohm, *Metal-to-Glass Vacuum Seal for Low Temperatures.* Review of Scientific Instruments, 1961. **32**(7): 857-858.
19. Sparks, D., S. Massoud-Ansari, and N. Najafi, *Long-term evaluation of hermetically glass frit sealed silicon to Pyrex wafers with feedthroughs.* Journal of micromechanics and microengineering, 2005. **15**(8): 1560.
20. Fang, Y., et al., *Experimental validation of a numerical model for heat transfer in vacuum glazing.* Solar Energy, 2006. **80**(5): 564-577.
21. Mackerle, J., *Finite element modelling of ceramics and glass, an addendum–a bibliography (1998-2004).* Engineering computations, 2005.
22. Fang, Y., et al., *Comparison of vacuum glazing thermal performance predicted using two-and three-dimensional models and their experimental validation.* Solar Energy Materials and Solar Cells, 2009. **93**(9): 1492-1498.
23. Piccolo, A., et al., *Energy performance of an electrochromic switchable glazing: Experimental and computational assessments.* Energy and Buildings, 2018. **165**: 390-398.
24. Collins, R. and T. Simko, *Current status of the science and technology of vacuum glazing.* Solar Energy, 1998. **62**(3): 189-213.
25. Zhu, Q., et al., *Finite element analysis of heat transfer performance of vacuum glazing with low-emittance coatings by using ANSYS.* Energy and Buildings, 2020. **206**: 109584.
26. Kocer, C. *The thermal and mechanical performance of a vacuum insulating glazing*. in *GLASS PERFORMANCE DATS 2015*. June 24-26, 2015. Tampere, Finland.
27. Cuce, E. and P.M. Cuce, *Vacuum glazing for highly insulating windows: Recent developments and future prospects.* Renewable and Sustainable Energy Reviews, 2016. **54**: 1345-1357.
28. Hart, R.H.a.C., D.C. *Modeling of Vacuum Insulating Glazing*. in *Proceedings of the Thermal Performance of Building Envelopes XII*. December, 2013. Clearwater Beach, Fl.
29. Hart, R.a.C.C., *Modeling of Vacuum Insulating Glazing*, in *Thermal Performance of the Exterior Envelopes of Whole Buildings XII International Conference*. 2013, ASHRAE.
30. Han, Z.M., et al. *Evaluation of thermal performance for vacuum glazing by using three-dimensional finite element model*. in *Key Engineering Materials*. 2012. Trans Tech Publ.
31. Islam, M.R. and A. Pramila, *Thermal conductivity of fiber reinforced composites by the FEM.* Journal of Composite Materials, 1999. **33**(18): 1699-1715.

32. *ABAQUS 3DEXPERIENCE R2017x*, Dassault Systemes SIMULA Corp., Johnston, RI, 2017.

33. Wang, J., et al., *Machine learning for thermal transport analysis of aluminum alloys with precipitate morphology.* Advanced Theory and Simulations, 2019. **2**(4): 1800196.

34. ASTM C1199-14, *Standard Test Method for Measuring the Steady-State Thermal Transmittance of Fenestration Systems Using Hot Box Methods.* ASTM International: West Conshohocken, PA, 2014.

35. ASTM E2188-19, *Standard Test Method for Insulating Glass Unit Performance*, ASTM International, West Conshohocken, PA, 2019.

36. ASTM E2190-19, *Standard Specification for Insulating Glass Unit Performance and Evaluation*, ASTM International, West Conshohocken, PA, 2019.

37. Corruccini, R., *Gaseous heat conduction at low pressures and temperatures.* Vacuum, 1959. **7**: 19-29.

38. Collins, R. and S. Robinson, *Evacuated glazing.* Solar Energy, 1991. **47**(1): 27-38.

39. Collins, R. and A. Fischer-Cripps, *Design of support pillar arrays in flat evacuated windows.* Australian Journal of Physics, 1991. **44**(5): 545-564.

40. Charlie Curcija, S.V., Robert Hart, Jacob Jonsson,Rebecca Powles,Robin Mitchell, *WINDOW Technical Documentation*. 2018: Windows and Envelope Materials Group, Lawrence Berkeley National LaboratoryBerkeley, California 94720.

41. ASTM, C518 *Standard Test Method for Steady-State Thermal Transmission Properties by Means of the Heat Flow Meter Apparatus.* 2017.

42. *Glass in building — Vacuum insulating glass — Part 1: Basic specification of products and evaluation methods for thermal and sound insulating performance.* ISO 19916-1:2018.

43. Makishima, A. and J.D. Mackenzie, *Calculation of bulk modulus, shear modulus and Poisson's ratio of glass.* Journal of Non-crystalline solids, 1975. **17**(2): 147-157.

44. Van Den Bergh, S., et al., *Window spacers and edge seals in insulating glass units: A state-of-the-art review and future perspectives.* Energy and Buildings, 2013. **58**: 263-280.

45. Jarimi, H., et al., *Design, mathematical modelling and experimental investigation of vacuum insulated semi-transparent thin-film photovoltaic (PV) glazing.* Journal of Building Engineering, 2020. **31**: 101430.

46. Fang, Y., et al., *Indium alloy-sealed vacuum glazing development and context.* Renewable and Sustainable Energy Reviews, 2014. **37**: 480-501.

47. Memon, S. and P.C. Eames, *Design and development of lead-free glass-metallic vacuum materials for the construction and thermal performance of smart fusion edge-sealed vacuum glazing.* Energy and Buildings, 2020. **227**: 110430.

48. Kerschbaumer, R.C., et al., *Comparison of steady-state and transient thermal conductivity testing methods using different industrial rubber compounds.* Polymer testing, 2019. **80**: 106121.

49. ISO 527-1:2019, *Plastics — Determination of tensile properties.*

VITA

Wenyuan Zhu was born in Quanzhou, Fujian Province in China. He started his undergraduate study in Xiamen University in 2015 at Fujian, China, and graduated with a bachelor's degree in Mechanical engineering in 2019. He started his graduate study at the University of Tennessee at Knoxville in 2019 as a Master student, focusing on heat transfer filed.